UCRL-10205

# University of California

# Ernest O. Lawrence Radiation Laboratory

TWO-WEEK LOAN COPY

*This is a Library Circulating Copy which may be borrowed for two weeks. For a personal retention copy, call Tech. Info. Division, Ext. 5545*

## EXPERIMENTAL STUDY OF THE $K^+_{\mu 3}$ AND $K^+_{e3}$ DECAY MODES OF THE $K^+$ MESON

Berkeley, California

## DISCLAIMER

This document was prepared as an account of work sponsored by the United States Government. While this document is believed to contain correct information, neither the United States Government nor any agency thereof, nor the Regents of the University of California, nor any of their employees, makes any warranty, express or implied, or assumes any legal responsibility for the accuracy, completeness, or usefulness of any information, apparatus, product, or process disclosed, or represents that its use would not infringe privately owned rights. Reference herein to any specific commercial product, process, or service by its trade name, trademark, manufacturer, or otherwise, does not necessarily constitute or imply its endorsement, recommendation, or favoring by the United States Government or any agency thereof, or the Regents of the University of California. The views and opinions of authors expressed herein do not necessarily state or reflect those of the United States Government or any agency thereof or the Regents of the University of California.

Research and Development

UCRL-10205
UC-34 Physics
TID-4500 (17th Ed.)

UNIVERSITY OF CALIFORNIA
Lawrence Radiation Laboratory
Berkeley, California

Contract No. W-7405-eng-48

# EXPERIMENTAL STUDY OF THE $K^+_{\mu 3}$ AND $K^+_{e3}$ DECAY MODES OF THE $K^+$ MESON

John L. Brown, John A. Kadyk, George H. Trilling,
Remy T. Van de Walle, Byron P. Roe, and Daniel Sinclair

August 20, 1962

# EXPERIMENTAL STUDY OF THE $K^+_{\mu 3}$ AND $K^+_{e3}$ DECAY MODES OF THE $K^+$ MESON

John L. Brown, John A. Kadyk, George H. Trilling,
and Remy T. Van de Walle

Lawrence Radiation Laboratory and Department of Physics
University of California, Berkeley, California

and

Byron P. Roe and Daniel Sinclair

Department of Physics
University of Michigan
Ann Arbor, Michigan

August 20, 1962

## ABSTRACT

To investigate the nature of strangeness-nonconserving weak interactions, we have examined a sample of 76 $K^+_{\mu 3}$ ($K^+ \rightarrow \mu^+ + \pi^0 + \nu$) and 216 $K^+_{e3}$($K^+ \rightarrow e^+ + \pi^0 + \nu$) decays at rest observed in a xenon bubble chamber. The combined data indicate that (1) the V-A theory correctly describes $K^+_{e3}$ and $K^+_{\mu 3}$ decay; (2) the $\mu^+$ and $e^+$ are coupled with the same strength in three-body leptonic $K^+$ decay; and (3) the magnitude and energy variation of the form factors involved are consistent with predictions based on the partially-conserved current hypothesis.

# EXPERIMENTAL STUDY OF THE $K^+_{\mu 3}$ AND $K^+_{e3}$ DECAY MODES OF THE $K^+$ MESON

John L. Brown, John A. Kadyk, George H. Trilling, and Remy T. Van de Walle†

Lawrence Radiation Laboratory and Department of Physics
University of California, Berkeley, California

and

Byron P. Roe and Daniel Sinclair

Department of Physics
University of Michigan
Ann Arbor, Michigan

August 20, 1962

## I. INTRODUCTION

### A. Theoretical Background

The basic idea of a universal Fermi interaction has been quite successful in predicting many of the observed features of weak interactions. At present it appears that a Fermi interaction restricted just to vector (V) and axial-vector (A) couplings is sufficient to explain much of the data on strangeness-conserving weak interactions. There has been much less exploration in the field of strangeness-nonconserving interactions. One area that offers the possibility for significant experimental tests is that of the three-body leptonic ($K_{L3}$) decays of the K meson: $K \rightarrow \mu + \pi + \nu$ ($K_{\mu 3}$) and $K \rightarrow e + \pi + \nu$ ($K_{e3}$). We have recently published in very brief form some of our experimental results coming from a study of $K^+$ decay into the above modes. This report is intended to describe the collection of data and to explain in detail the methods of analysis used.

The kinematics of $K_{\mu 3}$ or $K_{e3}$ decay in the K rest frame can be completely specified by two independent variables which we will choose initially to be P, the magnitude of the pion momentum, and $\theta$, the angle between the pion and neutrino momentum vectors. There is a third independent variable, the $\mu$ (or e) spin direction; since we are unable to observe this experimentally, the various theoretical distributions which follow represent averages over lepton spins. With suitable assumptions one can derive various joint distribution functions of the variables, P and $\theta$, for the various Fermi couplings. Among the assumptions made (some of which are implicit in the diagram of Fig. 1 for $K_{L3}$ decay) are

---

† Present address: Interuniversity Institute for Nuclear Science, Brussels, Belgium.

a. the leptons are produced at one vertex,

b. the weak interaction is considered to first order only,

c. there is no electromagnetic interaction between the pion and muon or electron,

d. the K spin is zero,

and

e. parity is conserved in the strong interactions (which occur inside the box in Fig. 1).

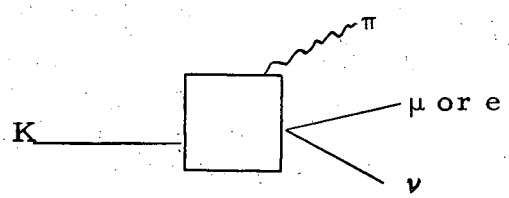


Fig. 1. Diagram for $K_{L3}$ Decay

In $K_{L3}$ decay one cannot distinguish between vector (V) and axial-vector (A) couplings, or scalar (S) and pseudoscalar (P) couplings. The usual convention is to take the vector, scalar, and tensor (T) couplings as those which might be present.

If one considers the case of pure couplings alone, one can derive the following distribution functions.[1]

Vector coupling

$$F_V(P,\theta)dP\,d\cos\theta = \frac{P^2}{E}\,\frac{(W^2 - P^2 - m_L^{\,2})^2}{(W + P\cos\theta)^4}\left\{P^2\sin^2\theta\, f_V^{\,2} + \frac{m_L^{\,2}}{M_K^{\,2}}\left[M_K f_V + (W + P\cos\theta)g_V\right]^2\right\} dP\,d\cos\theta; \quad (1a)$$

Scalar coupling

$$F_S(P,\theta)dP\,d\cos\theta = \frac{P^2}{E}\,\frac{(W^2 - P^2 - m_L^{\,2})^2}{(W + P\cos\theta)^2}\, f_S^{\,2}\, dP\,d\cos\theta; \quad (1b)$$

Tensor coupling

$$F_T(P,\theta)dP\,d\cos\theta = \frac{P^4}{M_K{}^2 E}\,\frac{(W^2 - P^2 - m_L{}^2)^2}{(W + P\cos\theta)^4}$$

$$\times\, f_T{}^2 \left[ (W\cos\theta + P)^2 + m_L{}^2 \sin^2\theta \right] dP\,d\cos\theta. \qquad (1c)$$

Here P is the pion momentum; E is the total pion energy; $\theta$ is the angle between the pion and the neutrino momentum vectors; $M_K$ is the K mass; $W = M_K - E$; $m_\pi$ and $m_L$ are the pion and lepton masses respectively; and $f_V$, $g_V$, $f_S$, and $f_T$ are functions ("form factors") of $q^2 = M_K{}^2 + m_\pi{}^2 - 2M_K E$, the square of the invariant four-momentum transfer. Although the theory does not require it, we have assumed time-reversal invariance of the weak interaction and have taken the form factors to be real.

One can try to determine experimentally if a single pure coupling (S, V, or T) is present in $K^+_{L3}$ decay by comparing the different $(P,\theta)$ distributions with the experimental data. The same type of coupling must be responsible for both $K^+_{e3}$ and $K^+_{\mu3}$ decay if we are to have a universal Fermi interaction. One can further ask if the data are consistent with $\mu$-e universality, wherein the coupling in $K^+_{e3}$ and $K^+_{\mu3}$ decay is not only of the same type but also of the same strength. As we will see later, our data can be described by a pure vector coupling of the same strength in both $K^+_{\mu3}$ and $K^+_{e3}$ decay.

Let us suppose now that a universal vector coupling is responsible for $K^+_{L3}$ decay. Examining Eq. (1a), we see that there are two form factors, $f_V$ and $g_V$, which are functions only of $q^2$ or equivalently of P. It should be noted that the term containing $g_V$ is multiplied by $(m_L/M_K)^2$ and hence is negligible in $K^+_{e3}$ decay. We will find that most theories predict $f_V$ and $g_V$ to be slowly varying functions of $q^2$, so that we can expand $f_V$ and $g_V$ in a power series in $q^2$ and keep only the first terms

$$f_V = A\left(1 + \lambda \frac{q^2}{m_\pi^2}\right) \qquad (2a)$$

and

$$g_V = B\left(1 + \lambda' \frac{q^2}{m_\pi^2}\right), \qquad (2b)$$

where A, B, $\lambda$, and $\lambda'$ are now parameters to be determined by experiment. Since $q^2/m_\pi^2$ ranges from roughly 0 to 7 in $K_{L3}$ decays, we may restrict $\lambda$ and $\lambda'$ to values less than, say, 0.1 in magnitude in order to keep within the spirit of a series expansion. As will be seen later, there is experimental justification for this, at least in the case of $\lambda$.

In order to predict the relative size of $g_V$ and $f_V$, or to predict their $q^2$ dependence, one must specify in some fashion what happens in the "box" in Fig. 1, i.e., say something about the strong interaction that connects the K and the $\pi$. This is usually done in the "current-current" formulation of the V-A theory.

In strangeness-conserving weak interactions, it appears that the vector current has zero divergence, i.e., is conserved.[2] A possible extension of this principle is to assume that the strangeness-nonconserving vector current is also conserved. This leads directly to a prediction for the ratio[3]

$$\frac{g_V}{f_V} = -\frac{M_K W}{q^2} \tag{3}$$

for a conserved vector current. This ratio varies from -1.4 to -10.6 over the range of $q^2$ allowed in $K^+_{\mu 3}$ decay.

More sophisticated theories using dispersion relations can lead to predictions for $f_V$ and $g_V$ separately. If one assumes that

a. $f_V$ and $g_V$ approach constants as $q^2 \to \infty$,

b. the dominant K-$\pi$ interaction is an S-wave resonance of mass $M_{K'}$,

c. the divergence of the strangeness-nonconserving current is a "gentle" operator (partially conserved vector current),

then one can show that[4]

$$f_V(q^2) \approx 2C,$$

and

$$g_V(q^2) \approx C\left[\frac{M_K^2 - m_\pi^2}{M_{K'}^2 - q^2} - 1\right],$$

where C is an unknown constant. In our notation this means

$$\lambda = 0$$

$$\lambda' = \frac{m_\pi^2}{M_{K'}^2} \quad \frac{(M_K^2 - m_\pi^2)}{(M_K^2 - m_\pi^2 - M_{K'}^2)} \quad , \tag{4}$$

and

$$B/A = \frac{1}{2} \quad \frac{M_K^2 - m_\pi^2 - M_{K'}^2}{M_{K'}^2}$$

for a partially conserved current, S-wave, K-$\pi$ resonance.

One can also derive[5] expressions for the form factors by replacing Eqs. (2) above by assuming that the dominant K-π interaction is a P-wave resonance of mass $M_{K''}$. The results in this case can be expressed in our notation as

$$\lambda = \lambda' = \frac{m_\pi^2}{M_{K''}^2} ,$$

and

$$\frac{B}{A} = -\frac{1}{2} \frac{M_K^2 - m_\pi^2 + M_{K''}^2}{M_{K''}^2} \tag{5}$$

for a partially conserved current, P-wave K-π resonance. Finally, one supposes that weak interactions are propagated by an intermediate vector boson of mass $M_B$. The predictions in this case[6] are the same as those in Eq. (5), with $M_{K''}$ replaced by $M_B$.

If we restrict ourselves to values of $M_{K'}$, $M_{K''}$, and $M_B$ greater than 600 MeV, Eqs. (4) and (5) lead to values of $|\lambda|$ and $|\lambda'|$ less than 0.08, and to values of B/A in the range -0.2 to -0.8.

## B. Previous Experimental Results

### 1. Test of the V-A Theory in $K^0_{e3}$ Decay

As mentioned earlier, one can test whether a single pure coupling is responsible for, say, $K^0_{e3}$ decay by comparing the various predicted $(P, \theta)$ distributions with experimental observations. In a hydrogen-bubble-chamber experiment with 124 identified $K^0_2 \rightarrow \pi^\pm + e^\mp + \nu$ events, Luers et al., on the basis of a comparison equivalent to that above, concluded that their data strongly favored the vector interaction.[7]

### 2. Muon Energy Spectrum in $K^+_{\mu 3}$ Decay

By transforming Eq. (1) from the variables $P, \theta$ to the variables $P, E_\mu$ ($E_\mu$ = muon total energy) and integrating over P, one can derive expressions for the muon energy spectra predicted by the various couplings with constant form factors. Emulsion studies have collected a certain amount of data on the $\mu^+$ energy spectrum in $K^+_{\mu 3}$ decay,[8] which have been insufficient to lead to any conclusion about the couplings involved.

If one assumes that a pure vector interaction is responsible for $K^+_{\mu 3}$ decay, and further assumes the form factors $f_V$ and $g_V$ to be constant, then the $\mu^+$ energy spectrum can be used to determine the ratio $g_V/f_V$. In a counter experiment using a filamentary chamber, Dobbs et al. determined the $\mu^+$ energy spectrum (for $E_\mu \geq 155$ MeV) on the basis of 139 events.[9] They concluded that either $g_V/f_V \geq +2$, or $g_V/f_V \leq -1.5$. This result is not in agreement with the predictions based on partially conserved vector currents [cf. Eqs. (4), (5)].[10]

## II. DATA COLLECTION

### A. Experimental Setup

The data described in this report were collected in a 12-in. diam., 10-in.-deep xenon bubble chamber exposed to a beam of positive K mesons having nominal momentum 700 MeV/c.[11] The beam was moderated to a momentum of about 450 MeV/c by gold absorbers placed just ahead of the chamber, causing the $K^+$'s to stop roughly in the center of the chamber. The beam produced an average of 2 to 3 $K^+$ decays per picture. The chamber has been described in detail elsewhere,[12] but the following relevant facts should be repeated.

a. The chamber has no magnetic field; however, because of the high stopping power of xenon, energy determinations can often be made from range measurements.

b. The average probability for a $\gamma$ ray from a $\pi^0$ decay to convert into an electron pair is about 70%.

c. The range of the $\mu^+$ from a $\pi^+$ decay at rest is only 1.3 mm., so that the characteristic $\pi^+ - \mu^+ - e^+$ decay chain cannot always be recognized.

### B. Scanning and Measurement

For convenience, the data used in this experiment were collected from three different samples of film, each scanned in a slightly different way. In all cases, the criteria for recognizing $K^+_{e3}$ and $K^+_{\mu 3}$ decays can be summarized as follows:

1. $K^+_{e3}$ decays -- a $K^+$ decay with two associated electron pairs and with a single charged secondary identified as an electron either by its multiple scattering or by its production of an electron shower.

2. $K^+_{\mu 3}$ decays -- a $K^+$ decay with two associated electron pairs and a single charged secondary which stopped and decayed in the chamber without undergoing a nuclear interaction. This latter requirement enabled us in scanning the events, to eliminate the vast majority of the more numerous $K^+_{\pi 2}(K^+ \rightarrow \pi^+ + \pi^0)$ decays, whose secondaries seldom stop in the chamber unless they undergo a nuclear interaction. Furthermore, this restriction to events with stopping $\mu^+$'s enabled us to make a kinematic reconstruction of the events while still keeping over half of the total number of $K^+_{\mu 3}$ decays.

All candidates for $K^+_{e3}$ and $K^+_{\mu 3}$ decays were measured on digitized measuring projectors on three different stereo views, and the events were reconstructed in real space. The coordinates and directions thus obtained were used for kinematic analysis and the application of geometric criteria.

## C. $K^+_{e3}$ Sample

### 1. Geometric Criteria

Several geometric criteria were imposed on $K^+_{e3}$ decays, mainly to insure high scanning efficiency. The $K^+$-decay point was required to be inside a cylinder whose boundaries were 5 cm from every surface of the chamber. The conversion point of each of the $\gamma$-ray pairs was required to be at least 2 cm from every surface of the chamber. Since $\gamma$-ray directions were determined from measurements of the $K^+$-decay point and the conversion point, a lower limit of 3 mm was placed on the distance between these two points in order to insure a reasonably accurate measurement of these directions.

### 2. Kinematic Analysis

Because of the short radiation length (4 cm) of liquid xenon, bremsstrahlung is a very important source of energy loss for electrons. We are thus unable to measure the energy either of the electron secondary or the electron pairs in $K^+_{e3}$ decay, except in a rather qualitative way. This prevents us from kinematically reconstructing the events, so that we cannot directly compare our data with the various predicted $(P, \theta)$ distributions. As we will show in Sec. III-A, however, there is a strong correlation between P and $\phi$, the angle between the momentum vectors of the two $\gamma$'s from the $\pi^0$ decay. Further, for $K^+_{e3}$ decay, because of the small mass of the electron, the angle $\theta$ in Eq. (1) can equally well be interpreted as the angle between the electron momentum vector and the $\pi^0$ momentum vector. There is a strong correlation between the angle $\theta$ thus defined and $\theta'$, the angle between the electron momentum vector and the bisector of $\phi$. Thus, although we cannot determine P and $\theta$ kinematically, we can measure the closely correlated quantities $\phi$ and $\theta'$.

### 3. Events with Ambiguous Secondaries

In roughly 10,000 $K^+$ decays that were examined to produce a final $K^+_{\mu 3}$ sample of 76 events and a final $K^+_{e3}$ sample of 216 events, there was a small number of decays, the identification of whose secondaries was not entirely unambiguous. These events were scanned independently by two physicists; in every case where an identification could be made, the two conclusions were the same. There remained 10 events for which both physicists agreed a secondary identification could not be made; these events were not included in either the $K^+_{e3}$ or the $K^+_{\mu 3}$ sample.

### 4. Electron-Recognition Probability

The probability of recognizing an electron secondary from $K^+_{e3}$ decay depends on the electron energy and the potential path available to the electron. In this section we wish to show that the dependence of the recognition probability on electron energy has a negligible effect on the conclusions we draw from $K^+_{e3}$ decay.

We do this by first outlining how we derive the probability that an electron will be recognized after going a distance between X and X + dX. We call this probability distribution R(X)dX, when averaged over the electron energy spectrum of $K^+_{e3}$ decay. To find R(X), we first define the experimentally determinable function

$$R_1(X) = \frac{R(X)}{\int_0^{20\text{ cm}} R(X)dX} ,$$

where $R_1(X)dX$ is the probability that an electron recognized within 20 cm will be recognized in the interval X to X + dX, and 20 cm represents practically the upper limit to the available potential path for $K^+$ secondaries. $R_1(X)$ was determined from 74 $K^+_{e3}$ decays, for each of which the recognition distance (as estimated by a physicist-scanner) and potential path were known. We need to know next what fraction of all electrons are recognized in less than 20 cm, i.e., how many electrons would escape detection even with our longest available potential path. This we cannot measure experimentally but must predict theoretically from a model that describes the mechanism by which we recognize electrons. Let us suppose that, because of its severe multiple scattering, we recognize any electron that reaches some low energy $\epsilon$. Although $\epsilon$ is a parameter to be determined, we might expect, a priori, $\epsilon \lesssim 30$ MeV. Using this model for electron recognition, using simple phase space to predict the initial $K^+_{e3}$ electron energy spectrum, and using shower theory to describe electron energy loss, we can derive a theoretical expression for $R_1(X)$ in terms of the parameter $\epsilon$. We find that (a) the predicted $R_1(X)$ agrees excellently with our observation for $\epsilon$ = 18 MeV, and (b) with this value of $\epsilon$, only 0.4% of the $K^+_{e3}$ electrons escape detection in a potential path of 20 cm. The theoretically predicted R(X) is shown in Fig. 2. If we now integrate R(X) over the known potential path distribution for decay secondaries, we find that, overall, 90% of $K^+_{e3}$ electrons is detected.

Now we turn to the question of bias introduced by our method of recognizing electrons. Firstly, any bias cannot be large, since our average detection efficiency is 90%. Secondly, the dependence of recognition probability upon initial electron energy will be slight because of the severe fluctuations in energy loss caused by the shower process. Finally, many of our $K^+_{e3}$ conclusions are based solely on the $\pi^0$ momentum spectrum, which is affected only indirectly by biases in electron energy.

## 5. Energy Dependence of γ-Ray Conversion Probability

The conversion probability for a γ ray increases with γ-ray energy (see Fig. 3). Therefore high-energy $\pi^0$'s have a slightly greater chance of producing two electron pairs than do low-energy $\pi^0$'s. This effect can be estimated by calculating the probability that a $\pi^0$ will produce two electron pairs within a constant potential path of 10 cm, since we know that $\pi^0$ decay occurs isotropically in the center of mass and that the mean conversion length depends on γ energy. If this probability is calculated one finds that this bias reflects itself in a bias in λ (see Eq. 2a), so that λ appears less than it really is. The amount of the shift is

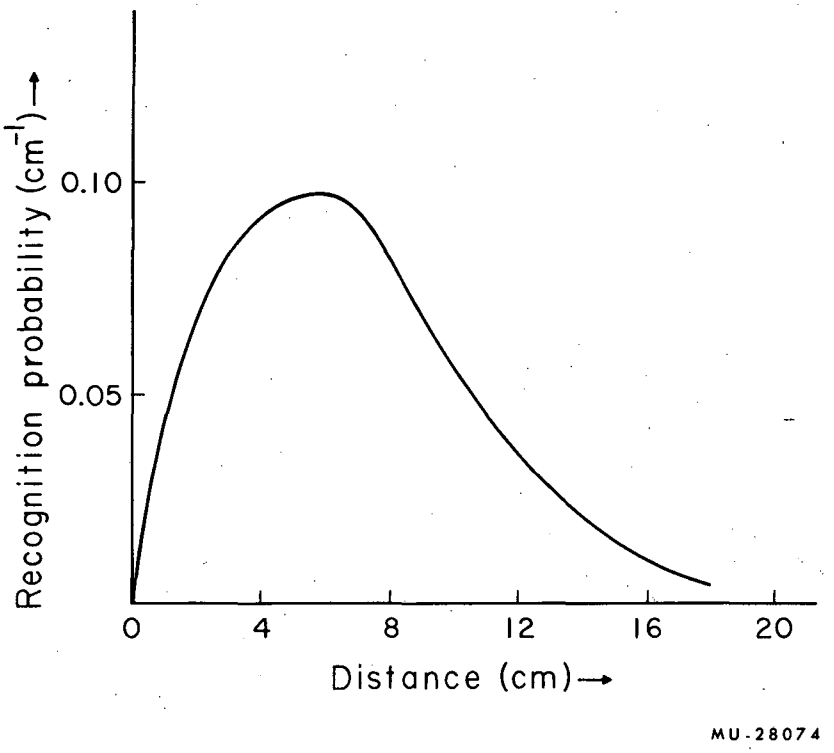


Fig. 2. Theoretical electron recognition probability, R(X), for $K^+_{e3}$ decays vs X.

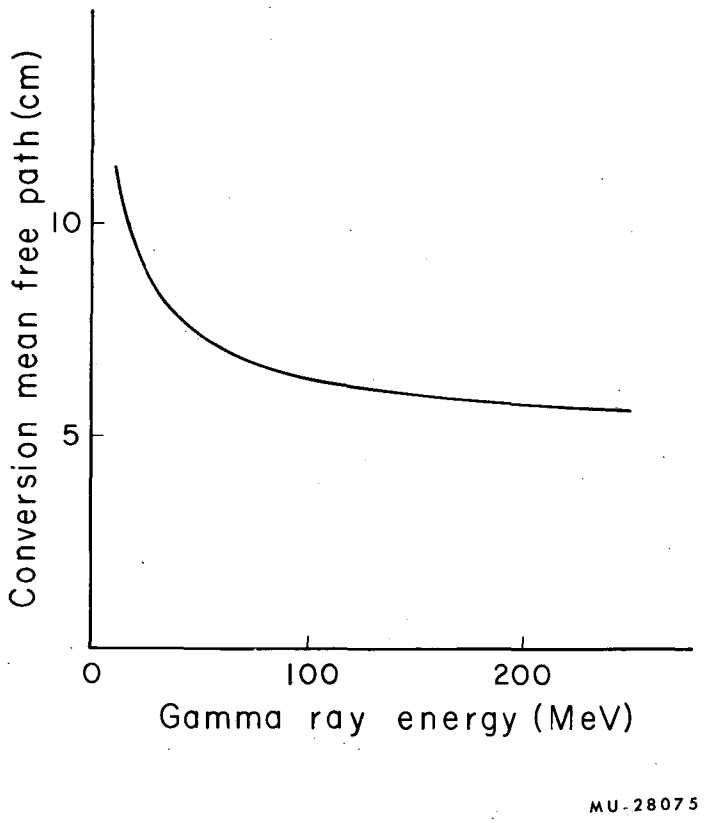


Fig. 3. Conversion mean free path for γ rays in liquid xenon as a function of γ-ray energy.

$$\delta\lambda \approx -4 \times 10^{-3},$$

which we shall see is small compared to our statistical uncertainty.

### 6. $K^+_{e3}$ Decays in Flight

A further bias in obtaining a $\pi^0$ momentum-distribution characteristic of $K^+_{e3}$ decays at rest comes from the inclusion of decays in flight. A $K^+$ decaying in flight with a short residual range ($\approx$ 3 cm) cannot be distinguished in scanning from a decay at rest. Knowing the moderation time as a function of residual range, we can estimate that about 2.5% of the events we call decays at rest in scanning are decays in flight, with momenta near 225 MeV/c; this means that in collecting 216 $K^+_{e3}$ decays at rest, we will also get about 5 $K^+_{e3}$ decays in flight. Some of these will be kinematically recognizable because the angle between the two $\gamma$-ray pairs will be less than the minimum possible (61.2 deg) from the highest energy $\pi^0$ (265-MeV total energy) that can be produced from a $K^+_{e3}$ decay at rest; in fact, two such events were found. This leaves about three completely unrecognized $K^+_{e3}$ decays in flight in our sample of 216; while this does constitute a bias, it is negligible compared to the inherent statistical error. Our $K^+_{e3}$ data is summarized in Appendix II.

## D. $K^+_{\mu 3}$ Sample

### 1. Geometric Criteria

All the geometric criteria applied to $K^+_{e3}$ decays were also applied to $K^+_{\mu 3}$ decay. In addition, the $\mu^+$ was required to have a range greater than 1 cm in order to prevent confusion with $K^+_{e3}$ decay.

### 2. Kinematic Analysis

The goal of the kinematic analysis of $K^+_{\mu 3}$ decay is to obtain values of P and $\theta$ (or more convenient, P and $E_\mu$) for each event, so that the experimental distributions of these quantities can be compared with the various theoretical predictions. We are able to reconstruct kinematically each $K^+_{\mu 3}$ event if we impose the restriction that the $\mu^+$ stop. The details of the reconstruction program will be found in Appendix I, but a brief outline will be given here.

First, it is clear that a reconstruction can be made; there are eight unknowns in the problem:

| | |
|---|---|
| $\vec{P}_\nu$, the neutrino momentum | 3 |
| $\vec{P}$, the pion momentum | 3 |
| $E_{\gamma 1}$, $E_{\gamma 2}$; the $\gamma$-ray energies | 2 |
| total | 8 |

and there are eight equations:

| | |
|---|---|
| conservation laws at the $K^+$-decay vertex | 4 |
| conservation laws at the $\pi^0$-decay vertex | 4 |
| total | 8 |

There is, however, one qualification. The reconstruction is double-valued; in particular, there are two $\pi^0$ momenta predicted and two sets of $\gamma$-ray energies. The $\mu^+$ total energy, directly determined from the range, is of course the same for both solutions. Frequently the two sets of $\gamma$-ray energies differ greatly; e.g., $E_{\gamma 1}$ = 40 MeV, $E_{\gamma 2}$ = 160 MeV for one solution, and $E_{\gamma 1}$ = 150 MeV, $E_{\gamma 2}$ = 30 MeV for the other. In these cases a crude measure of the total ionizing path length and potential path for the two electron pairs will allow one to pick the correct solution. In about one-third of the events, however, the solutions either differ very little in predicted $\gamma$ energies, or the available pair potential paths are too small to enable one to choose reliably the correct solution. In these cases we have chosen to average the two $\pi^0$ momenta. The error thus incurred is seldom much larger than the errors arising from measurement inaccuracies. The uncertainty in $\pi^0$ momenta due to both measurement error and averaging the two solutions when necessary, averaged over all events, is about 8 MeV/c.

It should be pointed out that not just any geometric configuration will permit a physically meaningful reconstruction. This follows from the fact that, in the reconstruction, one has to solve a quadratic equation for the square of the pion velocity. If the discriminant of this equation is positive, one gets two solutions, as discussed above. If, on the other hand, the discriminant is negative, then one obtains complex pion velocities, i.e., no solutions. Because of measurement error, a real $K^+_{\mu 3}$ decay at rest may fail to yield real pion velocities when kinematic reconstruction is attempted. To avoid "losing" real events for this reason, the reconstruction program calculates an expected error in the discriminant due to measuring inaccuracies. If a particular set of coordinates can be found differing from the measured ones by not more than a couple of standard deviations, such that the discriminant is positive, then the event is kept as real. This happened for six of the 76 $K^+_{\mu 3}$ events reported here. This is not unexpected when one notes that for 11 events whose nominal coordinates yielded real $\pi^0$ velocities, some reasonable perturbation of the nominal coordinates yielded complex velocities.

By means of this kinematic analysis one can derive a sample of $K^+$ decays, each with a stopping secondary and two electron pairs, and each of which "passes" the $K^+_{\mu 3}$ reconstruction program, i.e., is assigned real $\pi^0$ momenta. This by no means constitutes a pure sample of $K^+_{\mu 3}$ decays. We now proceed to discuss a number of sources of contamination.

3. $\tau'$ Contamination

The major source of contamination in our uncorrected data is $\tau'$ ($K^+ \rightarrow \pi^+ + \pi^0 + \pi^0$) decays in which two out of the four $\gamma$ rays convert. The $\pi^+$ from $\tau'$ decay almost invariably stops in the chamber, since its maximum range is only 8.2 cm. These stopping $\pi^+$'s cannot be reliably recognized by their characteristic $\pi^+$-$\mu^+$-$e^+$-decay chain, since the range of the intermediate $\mu^+$ is only 1.3 mm.

Since 2-$\gamma$ $\tau'$ events cannot be distinguished from $K^+_{\mu 3}$ events by scanning, we must seek some kinematic method of separation. As an aid to solving this problem, we generated 810 Monte Carlo $\tau'$ events. We assumed that phase space determines their decay configuration, and based their distribution throughout the chamber on the experimentally measured distribution of $K^+$-decay points. The 112 Monte Carlo events for which the $\tau'$ simulated $K^+_{\mu 3}$ decay--i.e., had two $\gamma$'s converting--were then processed by the $K^+_{\mu 3}$ reconstruction program. It was found that 27 events had secondary ranges less than 1 cm; these events were discarded immediately. About one-third of the remainder failed to give any real $\pi^0$ momenta, i.e., gave negative discriminants. About two-thirds did give real solutions. These would predict a contribution of about 20 events to our experimental $K^+_{\mu 3}$ sample, if no further restrictions were imposed. When these Monte Carlo events were examined, it was found that the distribution of the calculated cosine of the center-of-mass decay angle of the $\pi^0$,($\cos\theta^*$) was not isotropic, as one would expect for real $K^+_{\mu 3}$ events, but peaked strongly near $\pm 1$. This is shown in Fig. 4, where we have plotted the value of $\cos\theta^*$ associated with each of the two solutions for those Monte Carlo $\tau'$ events whose nominal coordinates "passed" the $K^+_{\mu 3}$ program. Each Monte Carlo event is represented twice in the histogram--once with $\cos\theta^* < 0$ (one solution) and once with $\cos\theta^* > 0$ (other solution). It is clear that if we discard $K^+$ decays whose secondary stops with a range less than 8.2 cm and for which $|\cos\theta^*|$ is calculated to be larger than 0.7, we will eliminate nearly all $\tau'$ events and rather few $K^+_{\mu 3}$ events (30% of those $K^+_{\mu 3}$'s with $\mu^+$ range less than 8.2 cm). Of the 112 Monte Carlo $\tau'$ 2-$\gamma$ events,

| | |
|---|---|
| 8 | events passed all $K^+_{\mu 3}$ criteria, |
| 29.5 | events failed the $K^+_{\mu 3}$ reconstruction program, |
| 47.5 | events passed the $K^+_{\mu 3}$ reconstruction program but had $\lvert\cos\theta^*\rvert > 0.7$, |

and

| | |
|---|---|
| 27 | events had secondary range < 1 cm. |
| 112 | |

Fractional events arise from events that nearly but do not quite pass, or have one solution with $|\cos\theta^*| > 0.7$, the other with $|\cos\theta^*| < 0.7$, etc. Using the known $\tau'$ branching ratio, the probability that two of the four $\gamma$'s convert, and the above results, one can calculate that our final sample of 76 $K^+_{\mu 3}$ decays contains about 3 $\tau'$ decays.

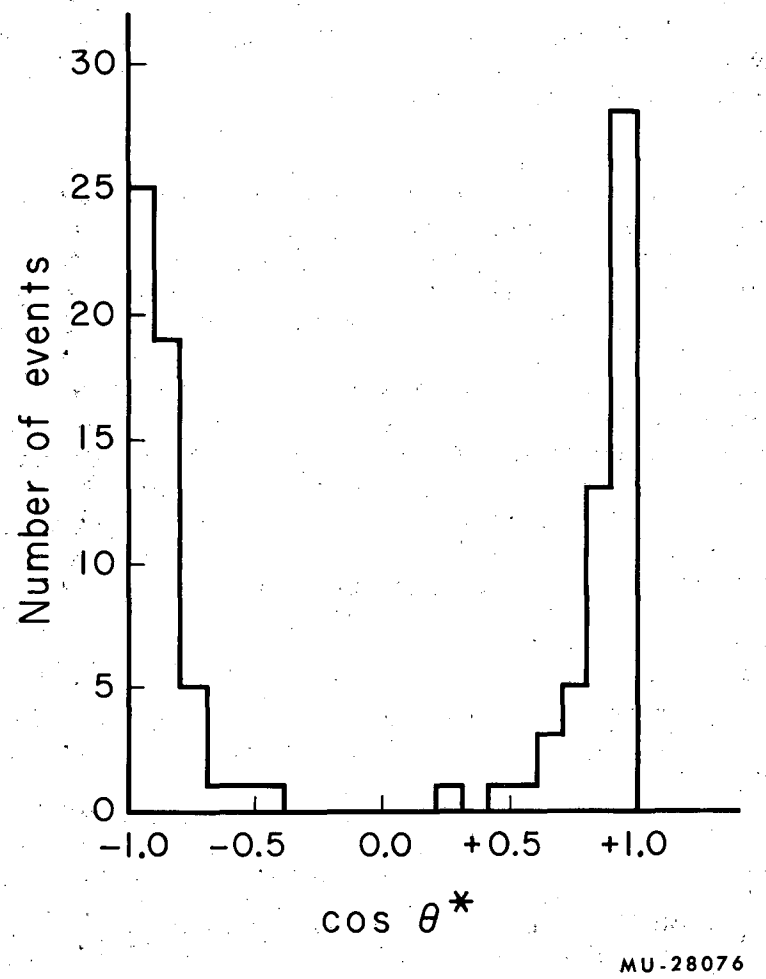


Fig. 4. Distribution of $\cos\theta^*$ for Monte Carlo $\tau'$ events reconstructed as $K^+_{\mu 3}$ decays.

4. $K^+_{\pi 2}$ Contamination

A second source of contamination (which can bias the $\pi^0$ momentum distribution) is $K^+_{\pi 2}$ events in which both $\gamma$'s convert and in which the $\pi^+$ undergoes an undetected nuclear interaction or decay in flight, causing it to stop in less than the characteristic range of 23.5 cm. Since about one out of every seven $\pi^+$'s from $K^+_{\pi 2}$ decay undergoes a nuclear interaction detectable at the scanning table, some small fraction may undergo a small-angle prongless inelastic nuclear interaction that causes the event to simulate a $K^+_{\mu 3}$ decay.

We can check whether this happens frequently by subjecting each $K^+_{\mu 3}$ candidate to the following kinematic checks appropriate to the $K^+_{\pi 2}$ decay at rest.

1. The plane defined by the two-$\gamma$ momentum vectors must also contain the charged secondary, within measurement errors.

2. The magnitude of the $\pi^0$ momentum, derived from the two measured $\gamma$ directions and the $\pi^0$ direction, which is assumed opposite to that of the charged secondary, must equal 205 MeV/c (the value expected for the $\pi^0$ in a $K^+_{\pi 2}$ decay at rest) within measurement errors.

Of the 76 finally accepted $K^+_{\mu 3}$ candidates, 10 passed the kinematic tests for a $K^+_{\pi 2}$ decay at rest (except of course for not having a 23.5-cm range). To see how many real $K^+_{\mu 3}$ events one would expect to pass $K^+_{\pi 2}$ decay at rest kinematics, we generated 2000 Monte Carlo $K^+_{\mu 3}$ events using approximately the final values of A, B, $\lambda$, and $\lambda'$, and subjected these to the $K^+_{\pi 2}$ tests. It was found that about 8% of accepted $K^+_{\mu 3}$'s pass $K^+_{\pi 2}$ kinematics; i.e., we would expect six in our sample of 76. Thus we estimate that perhaps $4 \pm 3$ events in our final sample might be $K^+_{\pi 2}$ decays at rest.

5. Decays in Flight

Another possible source of contamination is $K^+_{\pi 2}$ decays in flight. The $K^+_{\pi 2}$ decay mode represents about 19% of all $K^+$ decays.[13] As discussed earlier, about 2.5% of all $K^+$ decays which we call decays at rest are in fact decays in flight, usually with $K^+$ momenta near 225 MeV/c. To estimate how many would simulate $K^+_{\mu 3}$'s we generated a number of artificial $K^+_{\pi 2}$ decays in flight, choosing the decay configuration and $\gamma$-conversion points by a Monte Carlo process, and basing the decay points on a representative sample of measured $K^+$ decays. We found that 0.9% of all $K^+_{\pi 2}$ decays in flight at 200 MeV/c could be successfully reconstructed as $K^+_{\mu 3}$ decays at rest. Using the above figures and the fact that we scanned a total of about 10,800 $K^+$ decays, one can estimate that our sample of 76 $K^+_{\mu 3}$ decays contains less than one $K^+_{\pi 2}$ decay in flight.

A similar argument can be applied to the $K^+_{\mu 3}$ decay-in-flight contamination. Using the 2.5% estimate for the probability of a decay in flight, we might expect about two $K^+_{\mu 3}$ decays in flight in a sample of 76 accepted decays at rest. These $K^+_{\mu 3}$ decays in flight will tend to have higher laboratory $\mu^+$ energies (and hence less probability of stopping) and higher laboratory $\pi^0$ momenta (and hence a chance of completely failing the $K^+_{\mu 3}$ reconstruction program). Thus the actual contamination may be considerably less than two events; in any case, it is negligible.

## 6. Rare Decay-Mode Contamination

We have not made an exhaustive examination of the possibility that some of our alleged $K^+_{\mu 3}$ events may actually be examples of unusual $K^+$ decays. One possibility that comes to mind, however, is $K^+ \rightarrow \pi^+ + \pi^0 + \gamma$. In the sample of $K^+$ decays that produced 76 $K^+_{\mu 3}$'s, we found one example of an event with a long stopping secondary (R = 17.6 cm) and three electron pairs which passed the kinematic tests appropriate to the $\pi^+\pi^0\gamma$ mode. For every one of this type we might expect roughly two with only two electron pairs appearing, which could appear as another source of contamination in our $K^+_{\mu 3}$ sample. The frequency of this rare decay mode is probably not as high as this single possible event would indicate, however; a cursory examination of about 50,000 more $K^+$ decays failed to turn up any more cases with three electron pairs and a stopping secondary whose range was greater than that allowed in $\tau'$ decay, i.e., 8.2 cm. Thus the contamination from this source is probably negligible.

We can now summarize our sources of contamination in our sample of 76 alleged $K^+_{\mu 3}$ events as

| | | |
|---|---|---|
| $\tau'$ | decays | $\approx 3$, |
| $K^+_{\pi 2}$ | decays at rest | $\approx 4$, |
| $K^+_{\pi 2}$ | decays in flight | $< 1$, |
| $K^+_{\mu 3}$ | decays in flight | $< 2$, |

and

| | | |
|---|---|---|
| $\pi^+\pi^0\gamma$ | decays | $\approx 0$. |

Our final criteria that produced these 76 events are

a. the $K^+$ decay had to occur more than 5 cm from the chamber boundaries,

b. the secondary had to stop without a visible interaction,

c. both $\gamma$ rays had to convert into electron pairs more than 3 mm from the $K^+$ decay and more than 2 cm from the chamber boundaries,

d. the secondary range had to be greater than 1 cm,

e. the reconstruction program had to assign real momenta to the $\pi^0$, either for the measured coordinates or reasonable perturbations thereof,

f. if the secondary range was less than 8.2 cm, $|\cos\theta^*|$ had to be less than 0.7 for the chosen solution.

The data are summarized in Appendix III.

## III. ANALYSIS OF DATA

The present background of experimental and theoretical work has raised a number of questions that the study of the three-body leptonic modes of the $K^+$ is particularly well-suited to answer. Among the more important questions are

a. Of the various types of couplings--V, S, and T--is there one specific coupling that describes $\Delta S \neq 0$ interactions? (The V-A coupling seems to be correct for $\Delta S = 0$ processes.)

b. Does $\mu$-e universality apply to $\Delta S \neq 0$ reactions as well as to $\Delta S = 0$ reactions; i.e., are the $\mu$ and e coupled with equal strengths in $K^+$ decays?

c. What are the strengths of the form factors (coupling constants)? How do the strengths depend upon the pion momentum?

We will try to answer these questions by using the samples of 216 $K^+_{e3}$ decays and of 76 $K^+_{\mu 3}$ decays.

These two samples have been collected by using quite different selection criteria, because different sets of quantities are measured in the two decay modes. (See Sec. II-C and II-D.) For this reason, the analyses used on the two decay modes are quite different and will be discussed separately.

The most general description of three-body leptonic K-meson decay involves V, S, and T couplings (for pseudoscalar K), and also possible interference terms between these couplings. With the limited data available, we cannot investigate in detail the full range of possible coupling combinations. Instead, we will investigate only the pure couplings, V, S, and T. Until it can be shown that $\mu$-e universality is true for $K^+$ decays, we will affix a subscript e or $\mu$ to all quantities which in principle can be different in the $K^+_{\mu 3}$ and $K^+_{e3}$ decays.

### A. $K^+_{e3}$ Analysis

The decay distributions for V, S, and T for $K^+_{e3}$ decay are given in Eqs. (1a), (1b), and (1c). Since the electron mass is very small compared with other quantities occurring in the equations, all terms involving $m_L$ may be neglected for the case of $K^+_{e3}$ decay, and to this approximation, we find that the distribution is not changed if $\theta$ is taken to be the angle between the $e^+$ and $\pi^0$ instead of between the $\nu$ and $\pi^0$. We will use this fact in the analysis.

We can not measure the energy of the secondary electron or the energies of the $\gamma$ rays in xenon (except very crudely). Therefore, there is not enough measured information to reconstruct kinematically the $K^+_{e3}$ decay. To study the $\pi^0$ spectrum and ($\pi^0$, e) angular correlations predicted by Eqs. (1), we have instead investigated the distributions of two quantities closely correlated with those occurring in the theoretical distributions:

1. The angle $\phi$, the "opening angle" between the directions of the two $\gamma$-rays, , is a good statistical measure of the $\pi^0$ momentum. This is evident from Fig. 5, where the shapes of the $\pi^0$ spectra for V, S, and T are compared with corresponding shapes for the distributions of $\phi$. An average measurement error of 2 deg has been folded into the $\phi$ distribution. It is seen that the shapes of the distributions of P and $\phi$ are remarkably similar for any of the couplings shown, and there is not a very large "washout" due to the uncertainty of the decay angle in the $\pi^0$ decay.

2. The $\pi^0$-$e^+$ angular correlations were studied indirectly by measuring the distribution of the angle $\theta'$ between the direction of the $e^+$ and the direction of the bisector of $\phi$. The distribution of $\theta'$ is a close approximation to the distribution of $\theta$, and is particularly relevant to the discrimination between the various possible couplings. The quantities $\phi$ and $\theta'$ have the advantages that they can be measured readily and still retain most of the information available from the corresponding quantities P and $\theta$ in the theoretical distribution.

1. <u>Distribution of $\phi$</u>

For a given momentum, P, the $\phi$ distribution is given by

$$h(\phi)d\phi = \frac{m_\pi^2 \cot\frac{\phi}{2} \csc\frac{\phi}{2}\, d\phi}{2P(E^2 \sin^2\frac{\phi}{2} - m_\pi^2)^{1/2}} \quad . \tag{6}$$

For the distribution of $\phi$ resulting from the pion spectra, we fold Eq. (6) into Eqs. (1) and integrate out the pion momentum, which is not observable. Thus we have

$$H_e^i(\phi,\lambda_e)d\phi = \frac{1}{2}\, m_\pi^2 \cot\frac{\phi}{2} \csc\frac{\phi}{2}\, d\phi$$

$$\times \int_{m_\pi \cot\frac{\phi}{2}}^{P_{max}} \int_{-1}^{+1} F_e^{\,i}(P,\theta) \frac{d\cos\theta\, dP}{P(E^2 \sin^2\frac{\phi}{2} - m_\pi^2)^{1/2}} \quad , \tag{7}$$

where $F_e^i(p,\theta)$ are the distributions from Eqs. (1), with i = V, S, or T; and $P_{max} = 228.5$ MeV/c. The allowed kinematic limits on the range of $\phi$ are 61 to 180 deg.

The data were compared with the V, S, and T distributions, under the assumption that the form factors are constant. This is motivated by the theoretical expectation that the energy variation of the form factors is expected to be small. The distributions of $\phi$ resulting from V, S, and T couplings with constant form factors are

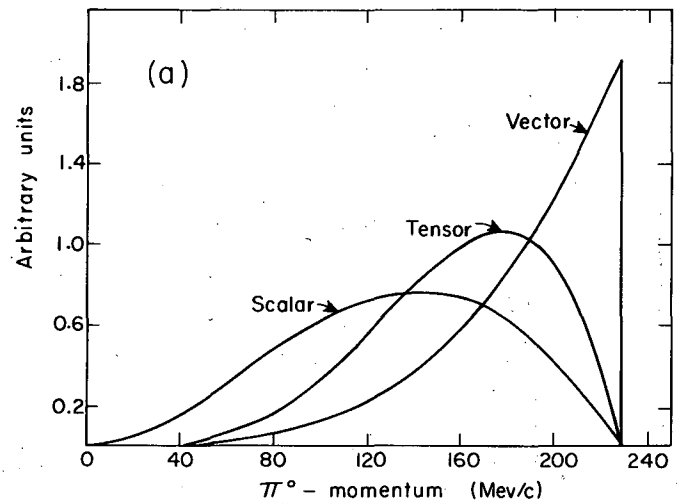


MU-24802

Fig. 5a. Pion momentum spectra for the various couplings. Constant form factors are assumed.

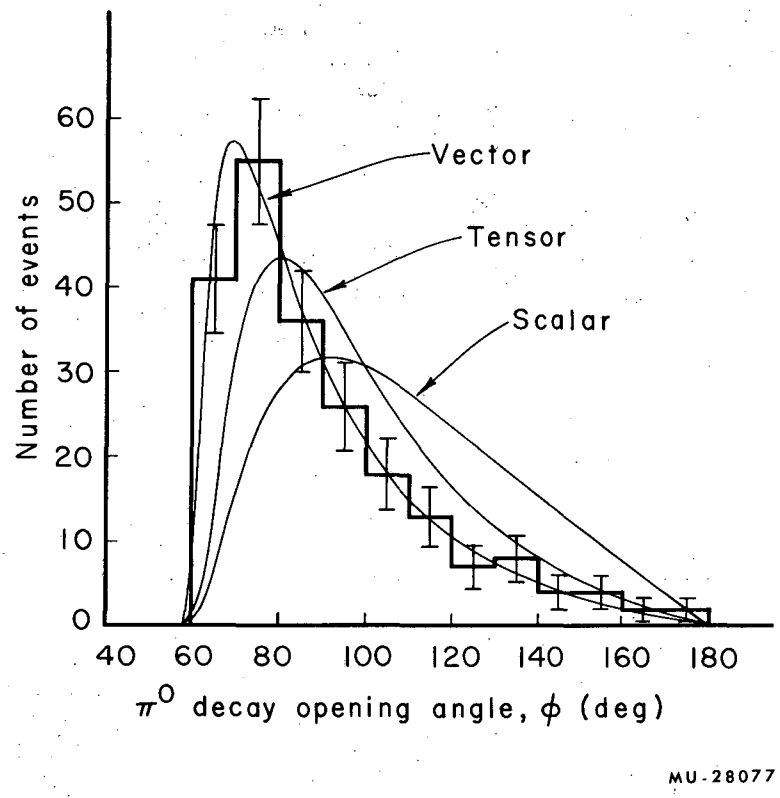


Fig. 5b. Experimental histogram and theoretical distributions for the $\pi^0$-decay opening angle $\phi$. Constant form factors are assumed.

vector: $H_e^V(\phi)d\phi = \frac{2}{3} f_V^2 m_\pi^4 \cot\frac{\phi}{2} \csc^2\frac{\phi}{2} (I_2 - I_0)\, d\phi;$

scalar: $H_e^S(\phi)d\phi = f_S^2 m_\pi^2 (M_K^2 + m_\pi^2) \cot\frac{\phi}{2} \csc^2\frac{\phi}{2} \left( I_0 - 2 \frac{M_K m_\pi}{M_K^2 + m_\pi^2} I_1 \right) d\phi;$

tensor:

$$H_e^T(\phi)d\phi = \frac{1}{3} f_T^2 m_\pi^4 \left(1 + \frac{m_\pi^2}{M_K^2}\right) \cot\frac{\phi}{2} \csc^2\frac{\phi}{2} \left[ I_2 - I_0 - 2 \frac{M_K m_\pi}{M_K^2 + m_\pi^2} (I_3 - I_1) \right] d\phi;$$

where

$$I_n = \csc^n\frac{\phi}{2} \int_1^{X_{max}} \frac{X^n dX}{\sqrt{X^2 - 1}}, \quad \text{where} \quad X_{max} = \frac{(P_{max}^2 + m_\pi^2)^{1/2}}{m_\pi} \sin\frac{\phi}{2}.$$

The average measurement error of 2 deg was folded into these distributions and compared with the observed distribution for $\phi$. The result is shown in Fig. 5 and in the following table of $\chi^2$ probabilities.

Table I. Goodness of fit of $\phi$ to V, S, and T distributions, $K_{e3}^+$

| Coupling | Degrees of freedom | $\chi^2$ | $\chi^2$ probability (%) |
|---|---|---|---|
| Vector | 12 | 10.5 | 55. |
| Scalar | 12 | 245.0 | < 0.1 |
| Tensor | 12 | 59.1 | <0.1 |

We conclude that scalar and tensor couplings are ruled out; the data agree quite well with vector coupling, for the case of constant form factors.

2. Distribution of $\theta'$

If an arbitrary energy variation of the form factors is allowed, one can always fit the data by a theoretical distribution for $\phi$ based on any of the couplings, though it would require a very large variation in the case of scalar coupling. For the angular distribution in $\theta'$, however, a test can be made which is independent of possible energy variation. This can be done by requiring the form factors to have an energy dependence such that the resulting $\phi$ distribution agrees with the observed data. The form factors are then fixed, within the statistical accuracy of the data, and the resulting angular correlations provide an absolute test of the various couplings.

Because of the mathematical difficulty of folding in the distribution of the bisector of $\phi$ to obtain the distribution of $\theta'$, we have used instead a Monte Carlo procedure, whereby a group of 1200 $K^+_{e3}$ decays were generated for each of the V, S, and T couplings and compared with the observed data. The three groups of events were all made with the $\pi^0$ momentum spectrum resulting from V coupling with a constant form factor, but with the angular distribution of $\theta$ appropriate to V, S, or T. This guarantees that the Monte Carlo events have a distribution in $\phi$ agreeing with the observed distribution, since the vector hypothesis was shown to give good agreement in the previous section. For each group of 1200 events, the distributions of the angle $\theta'$ are plotted in the form of histograms and compared with the observed distribution (see Fig. 6). It is evident that tensor coupling can be ruled out, but scalar can not. We find the agreement with the data, expressed in the form of $\chi^2$ tests, shown in Table II.

Table II. Goodness of fit of $\cos\theta'$ to modified V, S, and T distributions for $K^+_{e3}$

| Coupling | Degrees of freedom | $\chi^2$ | $\chi^2$ probability (%) |
|---|---|---|---|
| Vector | 9 | 8.1 | 50 |
| Scalar | 10 | 14.7 | 15 |
| Tensor | 11 | 61.2 | < 0.1 |

From these results we can conclude the following:

1. The data are consistent with the vector-coupling hypothesis. Within statistical accuracy, the form factor $f_V$ may be constant. Limits upon the energy variation of $f_V$ will be computed in the following discussion.

2. The data disagree with the tensor-coupling hypothesis for any choice of form factor.

3. If the scalar form factor is assumed to be slowly varying, the data disagree with the scalar hypothesis, but scalar coupling with a highly energy-dependent form factor cannot be ruled out.

## 3. Determination of $\lambda_e$

The previous discussion provides strong evidence that the correct form of coupling is vector. We now assume this to be true and compute the limits upon the energy variation of the form factor, consistent with a good fit to the observed $\phi$ distribution. Equation (7) for vector coupling, is integrated with the result

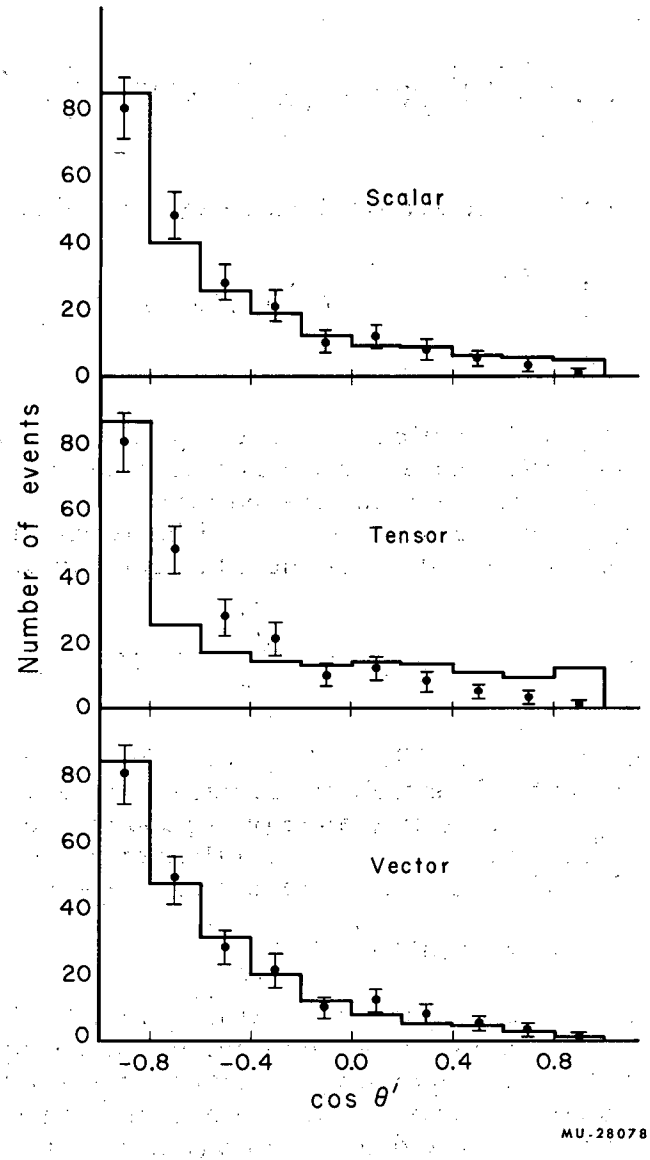


Fig. 6. Comparison between experimental and Monte Carlo $\cos\theta'$ distributions ($\theta'$ is the angle between the electron direction and the bisector of the angle $\phi$). The histogram represents the Monte Carlo results. The black circles with error flags represent our data.

$$H_e^V(\phi;\lambda_e)d\phi = \frac{1}{2}\frac{d\phi}{N_e(\lambda_e)}\cot\frac{\phi}{2}\csc^2\frac{\phi}{2}\left\{\left[m_\pi^2 + \lambda_e(M_K^2+m_\pi^2)\right]^2\left[I_2(\phi) - I_0(\phi)\right]\right.$$

$$\left. - 4M_K m_\pi \lambda_e\left[m_\pi^2 + \lambda_e(M_K^2+m_\pi^2)\right]\left[I_3(\phi) - I_1(\phi)\right] + 4M_K^2 m_\pi^2 \lambda_e^2\left[I_4(\phi) - I_2(\phi)\right]\right\} d\phi, \tag{8}$$

where $N_e(\lambda_e)$ is a normalization factor defined by the relation

$$A_e^2 N_e(\lambda_e) = \int_0^{P_{max}}\int_{-1}^{+1} F_e^V(P,\theta)d\cos\theta dP, \tag{9}$$

and $I_0, \ldots . I_4$ are as defined previously. An explicit evaluation of $N_e(\lambda_e)$ may be found in Appendix IV. Equation (8) is a function of the single experimentally observed variable $\phi$ and the parameter $\lambda_e$ to be determined. The value of $\lambda_e$ was found by the maximum likelihood procedure--by using a computer to calculate the logarithm of the likelihood from the data of 216 events:

$$\ell nL(\lambda_e, \phi_1, \ldots, \phi_{216}) = \sum_{i=1}^{216} \ell n\, H_e^V(\phi_i, \lambda_e).$$

In Fig. 7, $\ell nL$ is plotted vs $\lambda_e$. The value found for $\lambda_e$ is $0.034 \pm 0.045$, where the errors represent one-standard-deviation limits. A small correction must be made to $\lambda_e$ for the $\gamma$-ray energy dependence of conversion efficiency, which tends to increase the probability of observing both electron pairs for pions of higher energy. The corrected value is then

$$\lambda_e = +0.038 \pm 0.045.$$

The constant $A_e$ appearing in Eq. (2a) may now be found. It is related to the strength of the coupling between baryon and lepton currents, and will be compared with the corresponding constant for the $K^+_{\mu 3}$ decay, $A_\mu$, to test whether the muon and electron have equal coupling strengths, i.e., to test "$\mu$-e universality." We find $A_e$ by integrating Eq. (1) over the range of $\theta$ and P and equating the result to the known $K^+_{e3}$ rate, $R(K^+_{e3})$, which is known experimentally to be $(4.1 \pm 0.4) \times 10^6$/sec. From Eq. (9) we find

$$R(K^+_{e3}) = A_e^2 N_e(\lambda_e).$$

Since the $K^+_{e3}$ rate depends only on $\lambda_e$ and $A_e$, then $A_e$ may be considered as a function of $\lambda_e$. This dependence is shown in Fig. 8. However, the value for $\lambda_e$ quoted above is determined solely from the <u>shape</u> of the pion spectrum and may be used to determine

$$A_e = (7.0 \pm 0.8) \times 10^{-2}\ \mathrm{MeV}^{-2}\ \mathrm{sec}^{-1/2}.$$

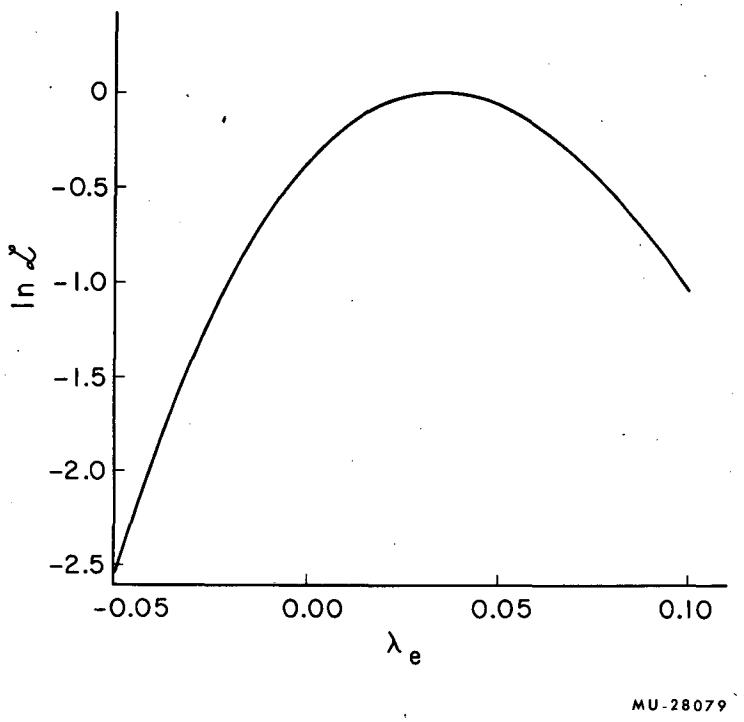


Fig. 7. Logarithm of likelihood function for $\lambda_e$ based on 216 $K^+_{e3}$ events.

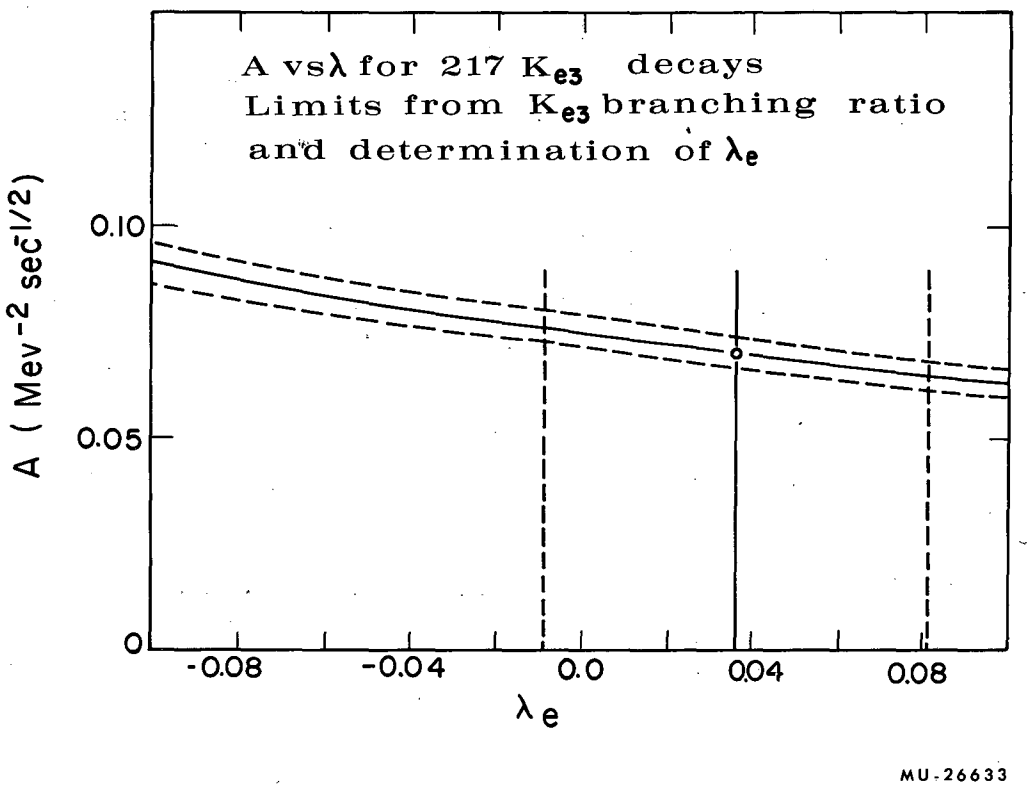


Fig. 8. Relation between A and λ. Horizontal solid and dashed curves are for nominal $K^+_{e3}$ rate and one-standard-deviation variation in rate. Vertical solid and dashed curves are for nominal λ and one-standard-deviation variation in λ, as determined experimentally from the $K^+_{e3}$ $\pi^0$ momentum spectrum.

The error on $A_e$ is due partly to the precision with which the $K^+_{e3}$ rate is known and partly to the determination of $\lambda_e$. The relative influence of these factors is also shown in Fig. 8 by the dashed lines representing one-standard-deviation limits.

## B. Distribution Functions for $K^+_{\mu 3}$ Data

In the $K^+_{\mu 3}$ decay, the decay kinematics for each event can be completely reconstructed if the muon stops in the chamber. However, there are several modifications that must be made in the theoretical distribution for the following reasons: (a) the xenon chamber is not large enough to stop the muon secondaries in all $K^+_{\mu 3}$ decays. About half of all of the $K^+_{\mu 3}$ decays will produce a muon of low enough energy that it will stop in the xenon. (b) When the secondary range is less than about 1 cm, the identification of the decay mode is ambiguous for certain events, and the range cannot be measured accurately. Therefore, the sample has been restricted to events having secondary ranges greater than 1 cm. (c) There is some contamination from $\tau'$ events when two of the four $\gamma$ rays convert. The criteria used for reducing this contamination are discussed in Sec. II. D. 3, and require the elimination of $K^+_{\mu 3}$ events when the muon range is less than 8.2 cm and $\theta^*$, the center-of-mass decay angle for the $\pi^0$, satisfies the relation $|\cos\theta^*| > 0.7$.

In order to modify the $K^+_{\mu 3}$ distribution functions to allow for these effects, the distributions in $(P, \cos\theta)$ given in Eqs. (1a), (1b), and (1c), were transformed to distributions in $(P, E_\mu)$ by the relation

$$\cos\theta = - \frac{W^2 - 2\,W\,E_\mu + m_\mu^2 + P^2}{2P(W - E_\mu)} .$$

The new distributions before modification are:

vector coupling:

$$G^V(P, E_\mu)dP\,dE_\mu = 2\,\frac{P}{E}\left\{\left[-4\,E_\mu^{\,2} + 4WE_\mu - (W^2 - P^2 - m_\mu^{\,2})\right] f_V^{\,2} + 4\,\frac{m_\mu^{\,2}}{M}\,(W - E_\mu) f_V g_V + \frac{m_\mu^{\,2}}{M^2}\,(W^2 - P^2 - m_\mu^{\,2})\,g_V^{\,2}\right\} dP\,dE_\mu , \qquad (10a)$$

scalar coupling:

$$G^S(P, E_\mu)dP\,dE_\mu = \frac{2P}{E}\,f_S^{\,2}\,(W^2 - P^2 - m_\mu^{\,2})dP\,dE_\mu , \qquad (10b)$$

tensor coupling:

$$G^T(P, E_\mu)dP\,dE_\mu = \frac{2P}{M_K{}^2 E} f_T{}^2 \left[P^2(W^2 - P^2 - m_\mu{}^2) - 4P^2(W - E_\mu)^2 + (W^2 + P^2 + m_\mu{}^2 - 2WE_\mu)^2\right] dP\,dE_\mu \quad . \tag{10c}$$

These distributions have two convenient features: (1) only one of the variables, P, depends upon the kinematic reconstruction, and the other, $E_\mu$, is a directly measured quantity; (2) the effect of the corrections can now easily be incorporated into the distribution by multiplying Eqs. (10a), (10b), and (10c) by $D(E_\mu)$, the a priori probability of observing an event with a stopping muon of energy $E_\mu$. The probability $D(E_\mu)$ was constructed as follows:

(a) A distribution of potential path lengths available to the secondary was found from measurement of the decay point and direction of the secondary in about 250 representative $K^+$-decay events. From this the basic geometric cutoff function, $D'(E_\mu)$, for the range of stopping muons was found. This is shown in Fig. 9.

(b) The function $D'(E_\mu)$ was modified by putting $D'(E_\mu) = 0$, where 105.7 MeV $\leq E_\mu \leq$ 120 MeV. This eliminates events with secondary ranges < 1 cm.

(c) The function $D'(E_\mu)$ was further modified by a decrease to 0.70 of its initial value in the interval 120 MeV $\leq E_\mu \leq$ 152 MeV to allow for events with $|\cos\theta^*| > 0.7$ discarded to remove $\tau'$ contamination. (See Sec. II. D. 3)

The form of the resulting distribution, $D(E_\mu)$, is shown in Fig. 10. The final distribution in $(P, E_\mu)$ for events observed satisfying the criteria imposed is found by multiplying $D(E_\mu)$ by each of the Eqs. (10).

## C. Analysis of $K^+_{\mu 3}$ Data - Universality Test

### 1. Evidence against S and T

The various coupling hypotheses can be tested by comparison of the $K^+_{\mu 3}$ data with the predictions of the distribution shapes. Since the form factors are not expected to have much variation with $\pi$ energy, we assume they are constant for the present. This assumption turns out to be compatible with the experimental results for the case of vector coupling. One convenient form in which to express the result is by means of the $\chi^2$ probability that the data fit the predictions for (1) the $\pi^0$ momentum spectrum, and (2) the $\mu^+$ energy spectrum. Table III gives the results of these $\chi^2$ tests.

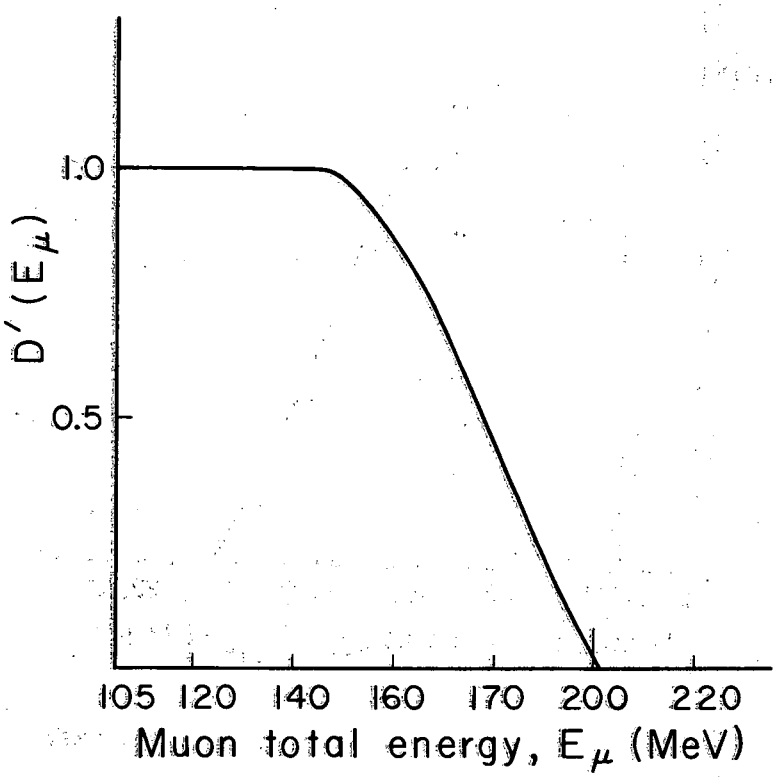


MU-28080

Fig. 9. Probability of muon stopping in chamber, $D'(E_\mu)$, as a function of muon total energy, $E_\mu$.

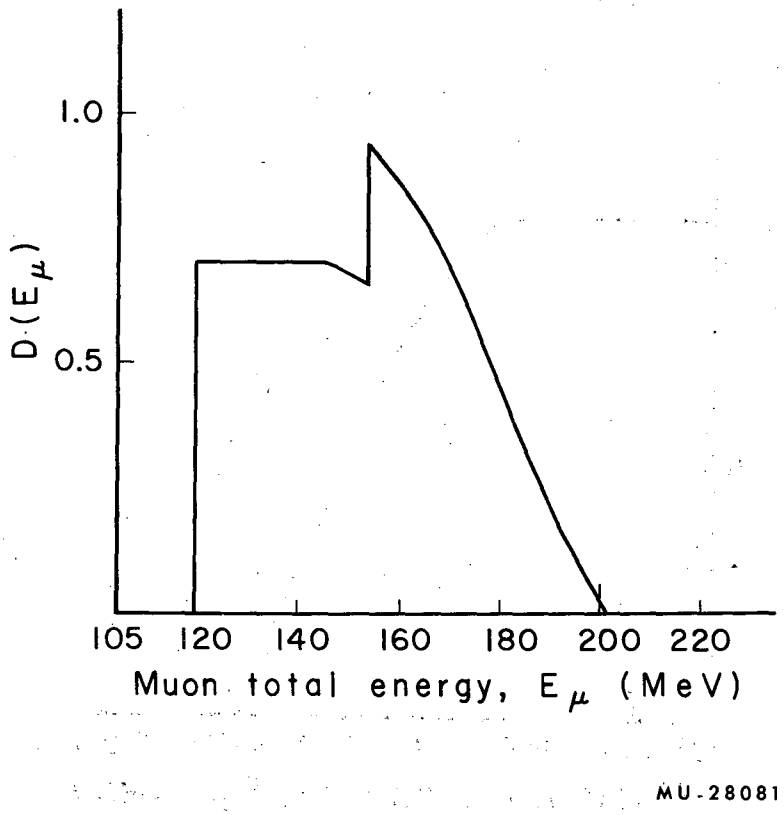


Fig. 10. Corrected probability, $D(E_\mu)$, of accepting muon from $K^+_{\mu 3}$ decay as a function of muon total energy, $E_\mu$.

of $A_\mu$ and $A_e$ are determined and can be compared. These determinations were made by using the maximum-likelihood procedure. The likelihood function, L, is expressed by:

$$\ell n\, L(P_i, E_{\mu i}; \lambda, A_e/A_\mu, \lambda'_\mu, B_\mu/A_\mu) = L' - \frac{[R_{exp} - R(\lambda, \lambda'_\mu, A_e/A_\mu, B_\mu/A_\mu]^2}{2(\Delta R_{exp})^2}, \tag{11}$$

where

$$L' = \sum_{i=1}^{76} \ell n \left[ N_\mu(\lambda, \lambda'_\mu, B_\mu/A_\mu) \right]^{-1} D(E_{\mu i}) G_\mu^V(P_i, E_{\mu i}; \lambda, \lambda'_\mu, B_\mu/A_\mu),$$

$$R_{exp} = \left( \frac{K^+_{e3} \text{ decay rate}}{K^+_{\mu 3} \text{ decay rate}} \right)_{experimental},$$

$$R = \left( \frac{K^+_{e3} \text{ decay rate}}{K^+_{\mu 3} \text{ decay rate}} \right)_{theoretical} = \left( \frac{A_e}{A_\mu} \right)^2 \frac{N_e(\lambda)}{N_\mu(\lambda, \lambda'_\mu, B_\mu/A_\mu)}, \tag{12}$$

$$A_\mu^2 N_\mu(\lambda, \lambda'_\mu, B_\mu/A_\mu) = \int_{m_\mu}^{E_{\mu max}} \int_{P_{min}(E_\mu)}^{P_{max}(E_\mu)} D(E_\mu) G_\mu^V(P, E_\mu; \lambda, \lambda'_\mu, B_\mu/A_\mu) dP\, dE_\mu,$$

and $N_\mu^V(\lambda, \lambda'_\mu, B_\mu/A_\mu)$ is a normalization factor for vector coupling, depending only upon chamber geometry and the masses of the particles involved. An explicit evaluation of $N_\mu$ can be found in Appendix IV. The first term in Eq. (11), L', represents the likelihood based entirely upon the shape of the $(P, E_\mu)$ distribution, while the second term imposes the constraint upon the ratio $A_\mu/A_e$ that the ratio of the experimentally observed $K^+_{e3}$ and $K^+_{\mu 3}$ rates be equal to the ratio determined by the parameters $\lambda \equiv \lambda_e \equiv \lambda_\mu$, $\lambda'_\mu$, and $B_\mu/A_\mu$. It turns out that the ratio $A_\mu/A_e$ is nearly independent of $\lambda_\mu$ and $\lambda'_\mu$:

$$\frac{A_\mu}{A_e} = 1.07 \pm 0.18.$$

Table III. $\chi^2$ probability of fit to S, T distributions, $K^+_{\mu 3}$

| | $\pi^0$ spectrum | | | $\mu^+$ spectrum | | |
|---|---|---|---|---|---|---|
| Coupling | Degrees of freedom | $\chi^2$ | $\chi^2$ probability (%) | Degrees of freedom | $\chi^2$ | $\chi^2$ probability (%) |
| Scalar | 5 | 81 | < 0.1 | 3 | 10.6 | 1.5 |
| Tensor | 4 | 7.9 | 9 | 4 | 10.4 | 4 |

Scalar coupling can be ruled out for a constant (or slowly varying) form factor, while tensor coupling seems unlikely, but cannot be ruled out. If an arbitrary energy variation of the form factors is allowed, then either the S or T predictions can be made compatible with the $K^+_{\mu 3}$ data.

Using these tests and the much stronger evidence from the $K^+_{e3}$ data as a basis, we will eliminate from consideration the possibilities of scalar and tensor couplings.

We will also give the $\chi^2$ probability of goodness-of-fit for the vector-coupling hypothesis, but here the procedure is somewhat more involved. While there was only one form factor in either the scalar or tensor distribution, there are two in the vector distribution, $f_V$ and $g_V$. Thus, for vector coupling, the distribution shape depends upon the ratio $g_V/f_V$, even if the form factors are constant, and to some degree the theory can be made to fit the data with an appropriate choice of $g_V/f_V$. However, if $\mu$-e universality is true, then the ratio of $K^+_{\mu 3}$- and $K^+_{e3}$-decay rates can be used to determine $g_V/f_V$, independently of the distribution shape. Therefore, we will try first, to prove that our data are consistent with the hypothesis of $\mu$-e universality, and if this is found to be so, we will use this fact to find $g_V/f_V$ from the known $K^+_{e3}$- and $K^+_{\mu 3}$-decay rates. Finally, we will test the compatibility of our data with the shape of the vector distribution by using the value of $g_V/f_V$ found from the rates.

## 2. Test of Universality

In the following discussion, we assume that there may be a small energy variation of the form factors as expressed by Eqs. (2). This way of expressing the energy variation is compatible with the predictions of all present theoretical models with the exception of the conserved-vector-current hypothesis, which will be discussed separately.

With sufficient numbers of events, it is possible in principle to determine the decay parameters $A_\mu$, $B_\mu$, $\lambda_\mu$, and $\lambda'_\mu$ from the $K^+_{\mu 3}$ data. Of these, $A_\mu$ and $\lambda_\mu$ can be compared with $A_e$ and $\lambda_e$, the corresponding quantities from $K^+_{e3}$ decay, to test $\mu$-e universality. However, the present sample of $K^+_{\mu 3}$ events is too small to make this possible. Instead, the following procedure is used. First, we take $\lambda_\mu \equiv \lambda_e \equiv \lambda$ and allow both $\lambda$ and $\lambda'_\mu$ to take any fixed value within their permissible range, $|\lambda| < 0.1$. We then allow $B_\mu/A_\mu$ to vary in order to fit the observed $K^+_{\mu 3}$ distribution shape as well as possible. From the $K^+_{\mu 3}$ and $K^+_{e3}$ decay rates, values

The error quoted is due to statistical uncertainties both in the determination of the branching ratio, $R_{exp}$, and in the $(P, E_\mu)$ distribution, and also due to the finite range of values allowed for $\lambda$ and $\lambda'$. This result was unchanged by small modifications in the distribution $D(E_\mu)$.

3. Best Values of A, B, and $\lambda$ from Combined Data

We now assume $\mu$-e universality to be valid because of the result of the previous test, and we can use both the $K^+_{\mu 3}$ and $K^+_{e3}$ data to find the best determinations of the various parameters. Since the $K^+_{\mu 3}$ distribution is quite insensitive to the values of $\lambda$ and $\lambda'$, $\lambda'$ cannot be found with reasonable precision, and the determination of $\lambda$ is made exclusively from the $K^+_{e3}$ data. The value of $A = A_\mu = A_e$ is then also found from the $K^+_{e3}$ decay rate by using the value of $\lambda$ determined by the distribution shape. The result, as determined in Sec. IV. A. is $\lambda = +0.038 \pm 0.045$ and $A = (7.0 \pm 0.8) \times 10^{-2}$ MeV$^{-2}$ sec$^{-1/2}$. From the observed $K_{\mu 3}$-to-$K_{e3}$ branching ratio, we now find B as a function of $\lambda'$ by using Eq. (12). The result is double-valued, because of the quadratic equations involved. The dependence of B on $\lambda'$ is shown in Fig. 11 in the form of two allowed bands, bounded by the dashed curves, which represent one-standard-deviation error limits in the $K^+_{\mu 3}$ decay rate. The solution for B near zero will henceforth be called Solution 1, while the other, which is large and negative, will be called Solution 2. However, these two solutions do not both fit the shape of the $(P, E)$ distribution. Solution 1 predicts the peak $\pi^0$ spectrum to be near high momentum and in the $\mu^+$ spectrum near low energy; for Solution 2 the positions of the peaks are reversed--the maxima occur at low $\pi^0$ momentum and high muon energy. To decide which solution is correct, we used the likelihood function L', which is independent of the $K^+_{\mu 3}$ and $K^+_{e3}$ rates, but dependent upon the shape of the $(P, E_\mu)$ distribution as determined by B and $\lambda'$. By maximizing L', we find B as a function of $\lambda'$. This is also plotted in Fig. 11 in the form of an allowed band bounded by the solid curves, which represent the error limits. Here we find that Solution 1 is quite compatible with this allowed band. Solution 2 is ruled out with a confidence exceeding 99.9%. It is also clear from the curves that the value of $\lambda'$ has little effect upon B for Solution 1, primarily because B is small; because of this, $\lambda'$ cannot be determined.

By combining the decay rates with the $(P, E_\mu)$ distribution, we find a best value of B from the likelihood function L, again assuming the values of A and $\lambda$ from the $K^+_{e3}$ analysis. The result is

$$B = 1.6 \times 10^{-2} \text{ MeV}^{-2} \text{ sec}^{-1/2}.$$

The errors in B are (a) uncertainties from the $K^+_{\mu 3}$ data, $\pm 2.4 \times 10^{-2}$ MeV$^{-2}$sec$^{1/2}$, and (b) uncertainties from the $K^+_{e3}$ data due to the determinations of $\lambda$ and the $K^+_{e3}$ rate. The error due to (b) is displayed in Fig. 12. It is difficult to assign a single error to B because the various sources of uncertainty are strongly correlated.

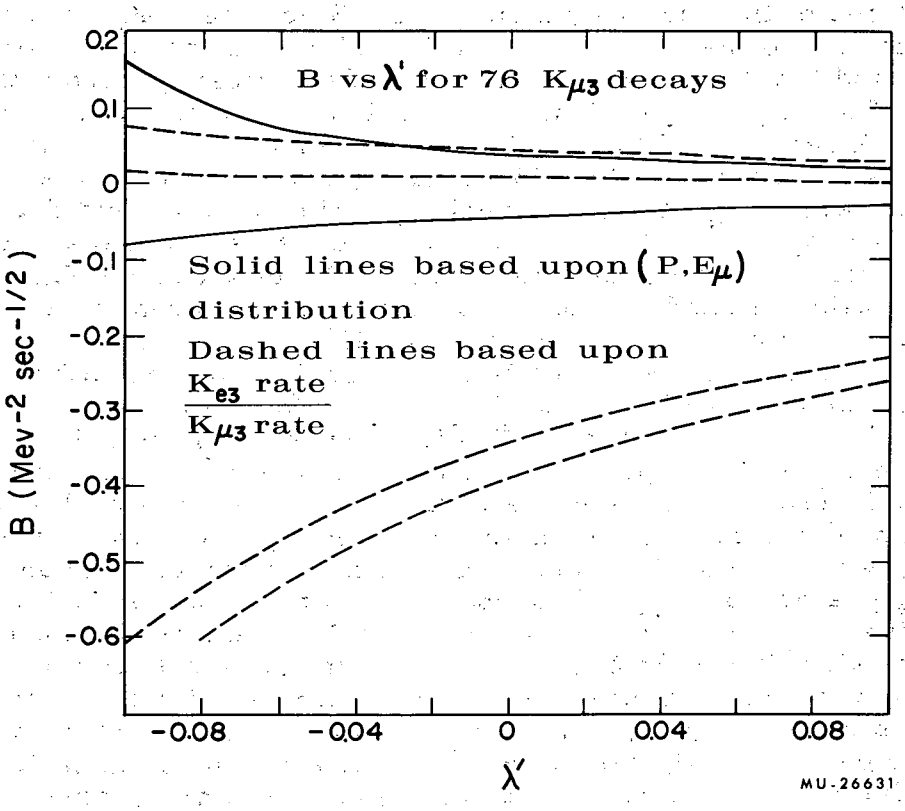


Fig. 11. Relation between B and λ' as determined from $K^+_{\mu 3}$ data. Dashed curves outline region allowed by one-standard-deviation variation in $K^+_{\mu 3}$ rate. Solid curves outline region allowed (at one standard-deviation level) by $K^+_{\mu 3}$ (P, $E_\mu$) distribution.

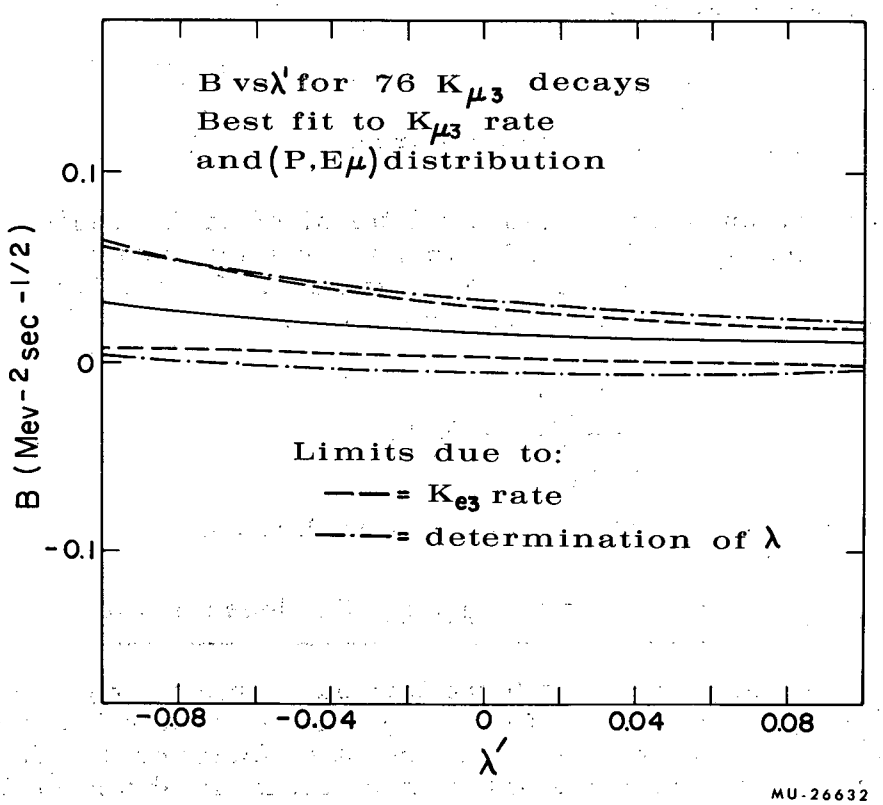


Fig. 12. Relation between B and λ' as determined from all the data. The solid curve represents the best value of B vs λ'. The dashed curve shows the effect of varying the $K^+_{e3}$ rate by one standard deviation; the dot-dash curve shows the effect of varying λ by one standard deviation.

4. Predictions of Theoretical Models

The results of this analysis have been compared with the predictions of various theoretical models--(1) conserved vector current, (2) partially conserved current and S- or P-wave (K-$\pi$) resonance, and (3) intermediate boson. The values predicted for B/A lie in the range -0.2 to -0.8, and the predictions for $|\lambda|$ lie between 0 and 0.08. With the exception of the conserved-vector-current hypothesis, our results are compatible with the predictions of all of these models.

The conserved-vector-current theory predicts a definite ratio $q_V/f_V$ that is strongly energy-dependent

$$\left(\frac{g_V}{f_V}\right)_{\text{conserved current}} = -\frac{M_K W}{q^2} .$$

Since the distribution shape is exactly determined in this model, it can be compared with the $K^+_{\mu 3}$ data. Such comparison shows that there is less than 2% $\chi^2$ probability of agreement. Furthermore, if $\mu$-e universality is assumed, the branching ratio is predicted to be

$$\frac{R(K^+_{\mu 3})}{R(K^+_{e3})} = 0.38.$$

This is incompatible with the observed ratio $0.96 \pm 0.15$.

D. Other Tests of $g_V/f_V$; Goodness of Fit

In the last section it was found that the solution for $g_V/f_V$ from the $K^+_{\mu 3}$ and $K^+_{e3}$ rates is double-valued. One of these solutions is near zero (Solution 1), and the other is large and negative (Solution 2). Solution 1 is quite compatible with the shape of the experimentally observed $(P, E_\mu)$ distribution, while the Solution 2 is strongly disfavored. However, because the experiment of Dobbs et al. led to the choice of Solution 2 as being correct, it is worthwhile to make whatever additional tests are possible on our data to see how well they actually do fit the solution we have adopted, and to see if there might be difficulties that have thus far escaped our notice and could have led to the wrong choice for $g_V/f_V$. These tests are also intended to reveal the extent to which the choice is sensitive to contamination of the $K^+_{\mu 3}$ sample and to the procedure used for finding the correct choice of kinematic solution in the $K^+_{\mu 3}$ reconstruction.

1. Contamination Studies

Among the known $K^+$-decay modes, only three can be sources of contamination to the $K^+_{\mu 3}$ sample, viz. $\tau'$, $K^+_{\pi 2}$, and $K^+_{e3}$. The criteria for reducing contamination have already been discussed in Sec. II. D. The $\tau'$ contamination is larger than either of the other two, unless the kinematic restrictions discussed in Sec. II. D. 3 are adopted. The $\tau'$ decays in the

sample constitute a bias in the direction of small $|g_V/f_V|$, both from the energy distribution of the charged secondary, which is obviously shifted to lower energies, and from the predicted $\pi^0$ momenta, which seems to occur mostly in the high-energy part of the spectrum when the $\tau'$-$2\gamma$ events are processed by the $K^+_{\mu 3}$ analysis. For these reasons, we calculated the $\pi^0$ momentum spectra expected in the intervals of $E_\mu$ corresponding to the secondary ranges above and below the maximum range for the $\tau'$ for each of the two solutions, $g_V/f_V$. This was done by integration of the predicted distributions over intervals in P chosen to constitute meaningful $\chi^2$ tests. By comparing these predictions with the data, we can find how sensitively the choice depends upon the data in the $\tau'$ range. The results of a $\chi^2$ test are found in Table IV. Thus, we see that nearly all the discrimination against Solution 2 comes from data that lies outside the $\tau'$ region. Therefore we conclude that the choice of $g_V/f_V$ is completely insensitive to the presence of $\tau'$ events in the sample, and the presence of the few such events expected cannot alter the decision.

## 2. Studies of $\pi^0$ Opening Angle Distribution

Another conceivable source of bias toward the incorrect choice is the procedure described in Sec. II. D. 2 for resolving the ambiguity of kinematic solutions for P. Although it is difficult to believe that this method could have led to a wrong result, one can still make a test which will be independent of the choice of P for the decays. This test consists of comparing the observed distribution of the opening angle, $\phi$, between the two $\gamma$-ray directions with the predictions based on the two solutions. The distribution in $\phi$ is found from the integration over the $\pi^0$ spectrum of the distribution for $\phi$ at a given momentum P. We obtain

$$H_\mu(\phi)d\phi = \frac{1}{2} m_\pi^2 \cot\frac{\phi}{2} \csc\frac{\phi}{2}\, d\phi \int_{m_\pi \cot\frac{\phi}{2}}^{P_{max}=215\ \mathrm{MeV/c}} \frac{g(P)dP}{P\left[E^2 \sin^2\frac{\phi}{2} - m_\pi^2\right]^{1/2}}$$

where g(P) is the $\pi^0$ momentum spectrum found by multiplying Eq. (10a) by $D(E_\mu)$ and integrating over $E_\mu$. Again, by integrating $H_\mu(\phi)$ over suitable intervals of $\phi$, we obtain convenient "bins" for a $\chi^2$ test (see Table V). Here we see that Solution 1 fits the data reasonably well, while Solution 2 is very strongly ruled out. We conclude that Solution 1 is the correct choice, independent of the procedure used for the kinematic reconstruction of the $K^+_{\mu 3}$ decays.

## 3. Goodness of Fit to the $E_\mu$ Distribution

We can also test the $E_\mu$ distribution against the two predictions. Here again the data were subjected to a $\chi^2$ test by integration of the predicted distribution over suitable "bins" (see Table VI). We find that the data fit Solution 1 remarkably well, whereas they are completely inconsistent with Solution 2.

Table IV. Goodness of fit of $\pi^0$ momentum spectra in certain $E_\mu$ intervals, $K^+_{\mu 3}$.

| $E_\mu$ range | $\Delta P$ (MeV/c) | Observed number of events | Solution 1: Predicted number of events | Solution 1: $\chi^2$ | Solution 1: Probability $\chi^2$ (%) | Solution 2: Predicted number of events | Solution 2: $\chi^2$ | Solution 2: Probability $\chi^2$ (%) |
|---|---|---|---|---|---|---|---|---|
| $< \tau'$ limit | 0-140 | 10 | 10 | | | 14.2 | | |
| | 140-170 | 10 | 11.5 | | | 10.6 | | |
| | 170-215 | 15 | 13.5 | | | 9.2 | | |
| | | | | 0.4 | 80 | | 4.9 | 9 |
| $> \tau'$ limit | 0-140 | 10 | 11.4 | | | 17.7 | | |
| | 140-170 | 9 | 11.7 | | | 11.9 | | |
| | 170-215 | 22 | 17.9 | | | 11.4 | | |
| | | | | 1.7 | 40 | | 13.9 | 0.4 |
| Entire range | 0-100 | 6 | 7.8 | | | 16.8 | | |
| | 100-140 | 17 | 18.9 | | | 23.6 | | |
| | 140-180 | 23 | 28.6 | | | 23.9 | | |
| | 180-215 | 30 | 20.7 | | | 11.7 | | |
| | | | | 5.9 | 12 | | 37 | < 0.1 |

Table V. Goodness of fit of $\phi$ distribution, $K^+_{\mu 3}$

| $\Delta\phi$ (deg) | Observed number of events | Solution 1 Predicted number of events | Solution 1 $\chi^2$ | Solution 1 $\chi^2$ probability (%) | Solution 2 Predicted number of events | Solution 2 $\chi^2$ | Solution 2 $\chi^2$ probability (%) |
|---|---|---|---|---|---|---|---|
| 60 to 80 | 22 | 16.6 | | | 9.6 | | |
| 80 to 100 | 29 | 26.7 | | | 23.1 | | |
| 100 to 120 | 15 | 17.2 | | | 20.3 | | |
| 120 to 180 | 10 | 15.5 | | | 22.9 | | |
| | | | 4.6 | 20 | | 25.8 | < 0.1 |

Table VI. Goodness of fit of $E_\mu$ distribution, $K^+_{\mu 3}$

| $\Delta E_\mu$ (MeV) | Observed number of events | Solution 1 Predicted number of events | Solution 1 $\chi^2$ | Solution 1 $\chi^2$ probability (%) | Solution 2 Predicted number of events | Solution 2 $\chi^2$ | Solution 2 $\chi^2$ probability (%) |
|---|---|---|---|---|---|---|---|
| 120 to 141 | 22 | 18.7 | | | 9.6 | | |
| 140 to 160 | 24 | 23.8 | | | 21.7 | | |
| 160 to 180 | 23 | 25.3 | | | 31.0 | | |
| 180 to 200 | 7 | 8.2 | | | 13.7 | | |
| | | | 1.0 | 80 | | 19.9 | < 0.1 |

From these various tests we find in each case that Solution 2 is strongly ruled out. The conclusion cannot be affected by the presence of $\tau'$ contamination, nor the procedure for picking the correct P from the double-valued kinematic solutions. Furthermore, we have seen that the goodness-of-fit tests are all in reasonable or good agreement with Solution 1.

## F. Discussion of Results and Summary

We find from the $K^+_{e3}$ analysis that pure vector coupling agrees well with the data, whereas tensor coupling can be ruled out for any energy variation of the form factor (from the $\pi$-e angular distribution). Scalar coupling can also be ruled out, providing there is not a very large energy variation of the form factor. Such variation would contradict all theoretical models presently considered. From the $K^+_{\mu 3}$ data, we find that there is good agreement with vector coupling. However, scalar coupling can only be ruled out if the form factor is constant or slowly varying, while tensor cannot be ruled out for even a constant form factor. However, the $K^+_{e3}$ data provide good evidence that scalar and tensor coupling cannot be present, and both $K^+_{e3}$ and $K^+_{\mu 3}$ data are quite compatible with vector coupling. Furthermore it is true that the data support the hypothesis of $\mu$-e universality for vector coupling.

The disagreement with the conclusions of Dobbs et al. cannot be understood on the basis of any internal inconsistency in the present data. Moreover, the various tests and checks which have been made seem only to corroborate the solution for $g_V/f_V$ that we have found.

Certain theoretical models predict the range of values that can be taken by B/A and $\lambda$, which are parameters of theoretical interest that can be found in this experiment. The range of values predicted for B/A lies between about -0.2 and -0.8, except for the conserved-vector theory, which we can rule out. This range of values is in reasonable agreement with the value we have found from the $(P, E_\mu)$ distribution alone $(+0.3 \pm 0.5)$, and is a little lower than the value we obtain from the ratio of $K^+_{\mu 3}$ and $K^+_{e3}$ decay rates $(+0.48 \pm 0.39)$, though not inconsistent over part of the range. The value found for $\lambda$ $(0.04 \pm 0.04)$ is also not inconsistent with the range of $\lambda$ predicted by the theories $(0 \leq \lambda \leq 0.08)$.

## ACKNOWLEDGMENTS

We wish to express our thanks to Dr. Donald A. Glaser, who first suggested the study of $K^+$ decay in a xenon bubble chamber. We also want to thank the members of the Lofgren Group, who made possible the experiment at the Bevatron.

This work was done under the auspices of the U. S. Atomic Energy Commission.

## APPENDIX I.

Table of Individual Events in the $K^+_{e3}$ Sample

| Event number | $\phi/2$ (deg)[a] | $\cos\theta'$ [b] | Event number | $\phi/2$ (deg) | $\cos\theta'$ |
|---|---|---|---|---|---|
| 29147 | 35.3 | -0.71090 | 38517 | 52.4 | -0.51446 |
| 1167 | 70.6 | +0.30614 | 38535 | 39.8 | -0.93967 |
| 6171 | 39.4 | -0.81648 | 3860 | 56.7 | +0.01932 |
| 28222 | 47.9 | -0.20250 | 3922 | 37.5 | -0.51059 |
| 28346 | 37.0 | -0.73084 | 25471 | 43.7 | -0.75439 |
| 28275 | 68.8 | -0.20503 | 38456 | 42.4 | -0.67612 |
| 35389 | 32.0 | -0.96813 | 28271 | 45.8 | -0.24807 |
| 35367 | 47.6 | -0.48491 | 28333 | 34.5 | -0.94636 |
| 1236 | 34.4 | -0.98078 | 28339 | 38.1 | -0.84994 |
| 20030 | 39.2 | -0.74145 | 3243 | 59.1 | -0.81617 |
| 20100 | 54.0 | -0.75146 | 38505 | 61.1 | -0.81087 |
| 28616 | 32.7 | +0.27198 | 5305 | 37.0 | -0.61961 |
| 39670 | 41.2 | -0.21207 | 33678 | 68.1 | +0.21847 |
| 35236 | 39.4 | -0.75747 | 33690 | 32.9 | -0.98280 |
| 35318 | 34.5 | -0.98016 | 33614 | 54.7 | -0.63544 |
| 28343 | 36.9 | -0.87379 | 33636 | 53.2 | -0.96594 |
| 39685 | 56.4 | -0.37542 | 5284 | 43.2 | -0.71814 |
| 28618 | 42.1 | -0.96348 | 33698 | 70.0 | +0.13685 |
| 8117 | 65.7 | -0.80740 | 33640 | 34.2 | -0.93314 |
| 8093 | 34.3 | -0.85402 | 3010 | 36.6 | -0.94840 |
| 4040 | 87.5 | -0.08518 | 3098 | 36.7 | -0.72348 |
| 28796 | 44.2 | -0.39258 | 5044 | 53.3 | -0.36933 |
| 5225 | 67.1 | +0.26487 | 5165 | 48.1 | -0.52471 |
| 25476 | 76.3 | -0.62512 | 3040 | 43.6 | -0.93057 |
| 4020 | 34.0 | -0.82883 | 3136 | 45.3 | -0.89231 |
| 39695 | 35.8 | -0.83895 | 5198 | 47.3 | +0.86020 |
| 3099 | 45.2 | +0.58009 | 6093 | 33.2 | -0.03702 |
| 3106 | 45.9 | +0.28771 | 4125 | 55.6 | -0.08375 |
| 5064 | 49.2 | -0.20460 | 33649 | 58.8 | -0.03073 |
| 5093 | 81.4 | +0.29110 | 28290 | 33.2 | -0.83994 |
| 5075 | 42.9 | -0.53198 | 39693 | 38.3 | -0.87553 |
| 5042 | 55.3 | +0.15303 | 29140 | 43.0 | -0.71874 |
| 9183 | 52.5 | -0.91201 | 28776 | 37.8 | -0.56080 |
| 9189 | 44.8 | -0.53800 | 38408 | 50.3 | -0.40714 |
| 38467 | 37.2 | -0.74010 | 2446 | 39.1 | -0.9010 |
| 2468 | 48.0 | -0.0009 | 50209 | 63.7 | +0.0529 |
| 2481 | 40.2 | -0.6148 | 50211 | 39.9 | -0.1278 |
| 2491 | 33.0 | -0.9835 | 50271 | 31.1 | -0.7333 |
| 2510 | 58.0 | -0.3792 | 50361 | 41.9 | -0.6619 |
| 2640 | 42.0 | -0.8034 | 17863 | 42.8 | -0.4687 |

| Event number | $\phi/2$ (deg) | $\cos\theta'$ | Event number | $\phi/2$ (deg) | $\cos\theta'$ |
|---|---|---|---|---|---|
| 2664 | 45.5 | -0.8764 | 16431 | 54.6 | +0.0834 |
| 2688 | 32.4 | -0.8734 | 25879 | 34.3 | -0.0285 |
| 2692 | 43.1 | -0.4296 | 19586 | 45.1 | +0.6687 |
| 2751-01 | 33.4 | -0.9310 | 19597 | 50.8 | -0.7349 |
| 2751-02 | 43.4 | -0.9949 | 20263 | 34.4 | -0.9525 |
| 2754 | 46.8 | +0.1064 | 20284 | 39.0 | -0.3198 |
| 2759 | 35.1 | -0.9841 | 38151 | 33.7 | -0.8952 |
| 2788 | 51.7 | +0.1825 | 38167 | 74.6 | -0.7887 |
| 5652 | 32.7 | -0.9985 | 19234 | 43.0 | -0.0986 |
| 5663 | 43.9 | -0.5788 | 19261 | 35.6 | -0.6034 |
| 5901 | 37.2 | -0.7236 | 19309 | 37.5 | -0.6686 |
| 24259 | 52.4 | -0.8399 | 19392 | 61.5 | -0.7313 |
| 24299 | 50.2 | -0.9795 | 19610 | 39.0 | -0.7881 |
| 24339 | 43.4 | -0.8347 | 19651 | 37.9 | -0.7310 |
| 24389 | 36.0 | -0.8258 | 19726 | 48.2 | -0.9596 |
| 24396 | 78.0 | -0.5271 | 46012 | 36.6 | -0.5413 |
| 25659 | 37.7 | -0.4396 | 46022 | 51.2 | -0.6567 |
| 24784 | 31.7 | -0.6245 | 46030 | 42.2 | +0.1995 |
| 24786 | 36.3 | -0.9511 | 46089 | 54.1 | -0.8648 |
| 29504 | 42.1 | -0.8593 | 1628 | 38.6 | -0.8310 |
| 29523 | 35.0 | -0.8026 | 19456 | 47.4 | -0.2495 |
| 26226 | 80.5 | -0.9144 | 19437 | 78.7 | +0.1087 |
| 26291 | 46.0 | -0.2399 | 50268 | 42.1 | -0.9346 |
| 26314 | 33.3 | -0.9956 | 50378 | 38.3 | -0.8572 |
| 34057 | 47.6 | -0.8555 | 46191 | 37.1 | -0.6208 |
| 34100 | 47.2 | -0.6739 | 37705 | 36.7 | -0.4430 |
| 34107 | 45.7 | -0.9521 | 37711 | 60.2 | -0.7733 |
| 34112 | 33.7 | -0.9626 | 6475 | 46.4 | +0.4337 |
| 6450 | 71.7 | -0.3699 | 17951 | 61.6 | -0.6383 |
| 6463 | 33.5 | -0.4689 | 16417 | 33.1 | -0.9828 |
| 6469 | 56.8 | -0.6477 | 46016 | 42.4 | -0.2510 |
| 6478 | 44.3 | -0.9768 | 46038 | 59.3 | +0.5562 |
| 6500 | 39.4 | -0.8522 | 46160 | 32.4 | -0.9832 |
| 7907 | 31.6 | -0.9244 | 19293 | 51.9 | -0.5095 |
| 7914 | 41.9 | -0.8136 | 19291 | 34.5 | -0.1921 |
| 17876 | 30.8 | -0.2337 | 20294 | 44.8 | -0.8071 |
| 25821 | 43.3 | +0.6757 | 37268 | 36.1 | -0.9578 |
| 25837 | 37.5 | -0.3426 | 17953 | 42.3 | +0.0803 |
| 37606 | 41.1 | -0.1984 | 19540 | 33.9 | -0.9933 |
| 37677 | 49.1 | -0.6759 | 19557 | 65.1 | +0.3834 |
| 37715 | 34.9 | -0.6682 | 19568 | 52.6 | -0.2893 |
| 38006 | 64.4 | +0.4357 | 19738 | 33.7 | -0.4393 |
| 38038 | 78.7 | +0.7875 | 19744 | 34.7 | -0.3431 |
| 38095 | 44.2 | -0.4708 | 37309 | 38.5 | -0.7840 |
| 38116 | 35.0 | -0.8838 | 37328 | 45.5 | -0.6616 |

| Event number | $\phi/2$ (deg) | $\cos\theta'$ | Event number | $\phi/2$ (deg) | $\cos\theta'$ |
|---|---|---|---|---|---|
| 38060 | 36.3 | -0.8605 | 8346 | 55.9 | -0.4322 |
| 38072 | 31.6 | -0.6329 | 8452 | 62.4 | -0.4924 |
| 38195 | 44.6 | -0.2880 | 8640 | 39.0 | -0.9126 |
| 50365 | 38.3 | -0.4993 | 8664 | 41.8 | -0.4289 |
| 2849 | 31.5 | -0.9984 | 8708 | 31.6 | -0.9796 |
| 3414 | 35.2 | -0.2510 | 8805 | 44.4 | -0.9171 |
| 3470 | 34.7 | -0.6677 | 8850 | 57.2 | -0.8321 |
| 3477 | 40.0 | -0.7532 | 8866 | 52.6 | +0.2915 |
| 3552 | 34.8 | -0.6533 | 8918 | 33.2 | -0.8906 |
| 3557 | 45.2 | -0.9764 | 8923 | 51.4 | -0.6116 |
| 4230 | 31.5 | -0.9898 | 46731 | 41.7 | +0.0036 |
| 4232 | 66.2 | +0.0899 | 46779 | 45.6 | -0.4178 |
| 4357 | 38.7 | -0.6545 | 17954 | 31.7 | -0.9757 |
| 4466 | 35.9 | -0.9221 | 37354 | 36.8 | -0.8573 |
| 4485 | 58.4 | -0.8429 | 38150 | 38.9 | -0.8959 |
| 4564 | 36.9 | -0.8292 | 5935 | 85.5 | -0.7027 |
| 6827 | 39.7 | -0.6704 | 19748 | 39.9 | -0.6339 |
| 6836 | 37.9 | -0.5705 | 37745 | 58.6 | -0.4567 |
| 6876 | 46.9 | -0.4303 | 38183 | 32.0 | +0.4394 |
| 7270 | 38.9 | -0.4644 | 2882 | 39.8 | -0.6240 |
| 7279 | 38.7 | -0.7595 | 2884 | 67.6 | -0.8637 |
| 7472 | 39.7 | -0.8925 | | | |
| 8215 | 67.2 | -0.2887 | | | |
| 8217 | 41.3 | -0.9501 | | | |
| 8282 | 47.5 | -0.6173 | | | |

[a] Here $\phi$ is the angle between two $\gamma$-ray momentum vectors.

[b] Here $\theta'$ is the angle between the electron momentum vector and the bisector of $\phi$.

# APPENDIX II

## $K^+_{\mu 3}$ Kinematic Reconstruction

### A. Definition of Symbols

$\vec{\gamma}_1$, $\vec{\gamma}_2$: unit vectors in the directions of the gamma rays

$\vec{\pi}$ : unit vector in the $\pi^0$ direction

$\vec{\mu}$ : unit vector in the $\mu$ direction

$\phi$ : $\cos^{-1} \vec{\gamma}_1 \cdot \vec{\gamma}_2$ = angle between the two gamma-ray directions

$\vec{P}_\mu$, $\vec{P}_\pi$, $\vec{P}_\nu$: momenta of $K^+_{\mu 3}$ secondaries

$\beta$ : $\pi^0$ velocity

$\gamma$ : $\frac{1}{\sqrt{1-\beta^2}}$ (not to be confused with $\vec{\gamma}_1$, $\vec{\gamma}_2$, defined above)

$E_\mu$, $E_\pi$ : $\mu$, $\pi^0$ total energies

$\xi$ : angle between the $\pi^0$ direction and the direction of $(\vec{\gamma}_1 + \vec{\gamma}_2)$

$E_{\gamma_1}$, $E_{\gamma_2}$ : $\gamma$-ray energies

$M_K$ : $K^+$ meson mass

$\theta^*$ : angle between $\pi$ direction and direction of $\gamma_1$ in center-of-mass of the $\pi^0$

$m_\pi$, $m_\mu$: pion and muon masses

### B. Detailed Calculation

We assume that we have a $K^+_{\mu 3}$ event in which the direction and energy of the $\mu$ are known (i.e., the $\mu$ stops in the chamber), and the directions of the two gamma rays from the $\pi^0$ decay are also known. Our goal is to calculate a complete reconstruction for the event.

We first define a convenient coordinate system related to the geometry of the event. Let

$$\vec{i} = \frac{\vec{\gamma}_1 + \vec{\gamma}_2}{|\vec{\gamma}_1 + \vec{\gamma}_2|} = \frac{\vec{\gamma}_1 + \vec{\gamma}_2}{2 \cos\frac{\phi}{2}} , \qquad \text{(II-1a)}$$

$$\vec{j} = \frac{\vec{\gamma}_1 - \vec{\gamma}_2}{|\vec{\gamma}_1 - \vec{\gamma}_2|} = \frac{\vec{\gamma}_1 - \vec{\gamma}_2}{2 \sin\frac{\phi}{2}}, \tag{II-1b}$$

$$\vec{k} = \vec{i} \times \vec{j} \ . \tag{II-1c}$$

With these definitions it is evident the $\pi$ direction can be written in the form

$$\vec{\pi} = \vec{i} \cos\xi + \vec{j} \sin\xi. \tag{II-2}$$

It is important to note that $\xi$ as used here has a definite sign, being positive if the $\pi^0$ makes the smaller angle with $\vec{\gamma}_1$, and negative if the $\pi^0$ makes the smaller angle with $\vec{\gamma}_2$. This point is essential when the gamma-ray energies are to be calculated.

We now also write

$$\vec{\mu} = \vec{i}\, a + \vec{j}\, b + \vec{k}\, c, \tag{II-3}$$

where, of course,

$$a = \vec{\mu} \cdot \vec{i}, \tag{II-4a}$$

$$b = \vec{\mu} \cdot \vec{j}, \tag{II-4b}$$

and

$$c = \vec{\mu} \cdot \vec{k}. \tag{II-4c}$$

We now apply the law of conservation of momentum

$$P_\nu^{\ 2} = (\vec{P}_\pi + \vec{P}_\mu)^2 = P_\pi^{\ 2} + P_\mu^{\ 2} + 2\, P_\pi\, P_\mu\, \vec{\mu} \cdot \vec{\pi},$$

$$= P_\pi^{\ 2} + P_\mu^{\ 2} + 2\, P_\pi\, P_\mu\, (a \cos\xi + b \sin\xi), \tag{II-5}$$

where we have used Eqs. (II-2) and (II-3).

Applying energy conservation, we find

$$P_\nu = M_K - E_\pi - E_\mu. \tag{II-6}$$

From Eqs. (II-5) and (II-6), we eliminate $P_\nu$ and obtain

$$(M_K - E_\pi - E_\mu)^2 = P_\pi^{\ 2} + P_\mu^{\ 2} + 2\, P_\pi\, P_\mu\, (a \cos\xi + b \sin\xi). \tag{II-7}$$

Now from $\pi^0$ decay kinematics we know that

$$\beta = \frac{\cos\frac{\phi}{2}}{\cos\xi} ;$$

hence

$$\cos\xi = \frac{\cos\frac{\phi}{2}}{\beta} \tag{II-8a}$$

and

$$\sin\xi = \frac{(\beta^2 - \cos^2\frac{\phi}{2})^{1/2}}{\beta} , \tag{II-8b}$$

Furthermore, we have $E_\pi = \gamma\, m_\pi$ and $P_\pi = \gamma\,\beta\, m_\pi$. Thus in Eq. (II-7) the only unknown quantity which appears is $\beta$, and Eq. (II-7) must be put in a form more tractable for calculating $\beta$. We rewrite Eq. (II-7) as

$$M_K^{\,2} + m_\pi^{\,2} + m_\mu^{\,2} - 2\, M_K\, E_\mu = 2\, E_\pi (M_K - E_\mu) + 2\, P_\pi\, P_\mu (a \cos\xi + b \cos\xi). \tag{II-9}$$

Now we define the symbol

$$U \equiv \frac{M_K^{\,2} + m_\pi^{\,2} + m_\mu^{\,2} - 2\, M_K\, E_\mu}{2\, m_\pi}, \tag{II-10}$$

which is directly calculable from measured data.

Then from Eqs. (II-8), (II-9), and (II-10), we have

$$U = \gamma(M_K - E_\mu) + P_\mu\, \gamma \left[ a \cos\frac{\phi}{2} + b\, (\beta^2 - \cos^2\frac{\phi}{2})^{1/2} \right] , \tag{II-11}$$

or

$$b\, (\beta^2 - \cos^2\frac{\phi}{2})^{1/2} = \frac{U}{P_\mu \gamma} - \lambda , \tag{II-12}$$

where

$$\lambda \equiv \frac{M_K - E_\mu}{P_\mu} + a \cos\frac{\phi}{2} \tag{II-13}$$

is again directly obtainable from measured data.

Squaring Eq. (II-12), we have

$$b^2\beta^2 - b^2 \cos^2\frac{\phi}{2} = \frac{U^2}{P_\mu^{\,2}} (1 - \beta^2) + \lambda^2 - \frac{2\,\lambda\, U}{\gamma\, P_\mu} ,$$

or

$$-\frac{2\lambda U}{\gamma P_\mu} = \beta^2\left(b^2 + \frac{U^2}{P_\mu^2}\right) - \sigma , \qquad \text{(II-14)}$$

where

$$\sigma \equiv b^2 \cos^2\frac{\phi}{2} + \left(\frac{U^2}{P_\mu^2}\right) + \lambda^2 \qquad \text{(II-15)}$$

is also directly related to the measured data.

Squaring Eq. (II-14), we have

$$\frac{4\lambda^2 U^2}{P_\mu^2}(1-\beta^2) = \beta^4\left(b^2 + \frac{U^2}{P_\mu^2}\right)^2 - 2\sigma\beta^2\left(b^2 + \frac{U^2}{P_\mu^2}\right) + \sigma^2 ,$$

or finally

$$\beta^4\left(b^2 + \frac{U^2}{P_\mu^2}\right)^2 + \beta^2\left(\frac{4\lambda^2 U^2}{P_\mu^2} - 2\sigma b^2 - 2\sigma\frac{U^2}{P_\mu^2}\right) + \sigma^2 - \frac{4\lambda^2 U^2}{P_\mu^2} = 0. \qquad \text{(II-16)}$$

This is a quadratic equation which, in general, leads to two solutions for $\beta^2$. Without discussing under what conditions this equation leads to physically acceptable solutions, we continue by assuming that a pair of real values of $\beta^2$ in the range $0 < \beta^2 < 1$ are obtained by solving Eq. (II-16). For each of these, we immediately calculate

$$P_\pi = \gamma\beta m_\pi ,$$

$$E_\pi = \gamma m_\pi ,$$

$$P_\nu \equiv E_\nu = M_K - E_\pi - E_\mu ,$$

and

$$\cos\xi = \frac{\cos\frac{\phi}{2}}{\beta} .$$

To calculate the directions of the pion and the neutrino and the gamma ray energies, we need $\sin\xi$ in magnitude and sign, i.e., we cannot just write $\sin\xi = (1 - \cos^2\xi)^{1/2}$. This is obtained from Eq. (II-5):

$$\sin\xi = \frac{P_\nu^2 - P_\pi^2 - P_\mu^2}{2 P_\pi P_\mu b} - \frac{a}{b}\cos\xi . \qquad \text{(II-17)}$$

Having this, we obtain the pion direction from Eq. (II-2) and the neutrino direction from

$$\vec{P}_{\nu} = - \vec{P}_{\pi} - \vec{P}_{\mu} . \qquad \text{(II-18)}$$

Finally, the cosine of the $\pi^0$ center-of-mass decay angle is given by

$$\cos \theta^* = \frac{\sin \xi}{\sin \frac{\phi}{2}} , \qquad \text{(II-19)}$$

where $\theta^*$ measures specifically the center-of-mass angle of $\gamma_1$. From Eq. (II-19) we readily calculate the two gamma-ray energies

$$E_{\gamma_1} = \frac{E_{\pi} + P_{\pi} \cos \theta^*}{2} , \qquad \text{(II-20a)}$$

and

$$E_{\gamma_2} = \frac{E_{\pi} - P_{\pi} \cos \theta^*}{2} . \qquad \text{(II-20b)}$$

## APPENDIX III

Table of Individual Events in $K^+_{\mu 3}$ Sample

| Event number | P (MeV/c)[a] | E (MeV)[b] | Event number | P (MeV/c) | E (MeV) |
|---|---|---|---|---|---|
| 2551 | 188.1 | 164.5 | 37316 | 130.9 | 149.7 |
| 2721 | 148.3 | 175.3 | 37327 | 101.6 | 164.5 |
| 2797 | 156.5 | 137.8 | 37339 | 175.5 | 162.1 |
| 5611 | 153.7 | 128.7 | 38104 | 188.4 | 126.4 |
| 5751 | 198.6 | 133.4 | 38143 | 199.0 | 153.6 |
| 5989 | 195.8 | 134.8 | 38159 | 201.2 | 140.9 |
| 24348 | 179.9 | 130.7 | 38196 | 143.1 | 126.9 |
| 24390 | 123.4 | 165.0 | 46105 | 181.5 | 159.6 |
| 24395 | 146.8 | 141.0 | 50248 | 192.5 | 142.7 |
| 24754 | 207.5 | 168.4 | 50281 | 182.4 | 157.2 |
| 24775 | 37.6 | 180.8 | 50348 | 147.6 | 166.2 |
| 25740 | 202.3 | 177.9 | 50356 | 132.1 | 147.1 |
| 26247 | 181.9 | 145.0 | 2890 | 170.0 | 128.9 |
| 26273 | 186.4 | 145.4 | 2944 | 171.4 | 124.0 |
| 29444 | 200.5 | 155.6 | 2971 | 118.2 | 158.8 |
| 34100 | 73.7 | 167.6 | 4279 | 191.1 | 141.9 |
| 34125 | 183.2 | 121.6 | 4373 | 160.7 | 139.6 |
| 34141 | 196.6 | 171.0 | 4409 | 123.4 | 127.4 |
| 34146 | 151.0 | 159.5 | 6991 | 130.9 | 121.9 |
| 34177 | 98.5 | 161.0 | 7342 | 164.4 | 156.6 |
| 1557 | 94.3 | 162.7 | 46634 | 205.3 | 156.2 |
| 7899 | 125.0 | 122.9 | 1061 | 174.1 | 182.4 |
| 16428 | 156.4 | 124.9 | 3132 | 183.7 | 138.1 |
| 17843 | 184.0 | 144.1 | 3163 | 73.9 | 159.3 |
| 17866 | 151.2 | 126.5 | 3236 | 161.0 | 190.4 |
| 19250 | 204.5 | 162.9 | 3291 | 183.3 | 184.9 |
| 19467 | 196.5 | 161.1 | 4184 | 130.0 | 167.5 |
| 19545 | 136.2 | 137.1 | 5288 | 183.7 | 169.0 |
| 19747 | 191.4 | 133.7 | 5301 | 127.1 | 126.2 |
| 20272 | 194.8 | 182.2 | 5370 | 208.6 | 178.2 |
| 20345 | 176.8 | 176.0 | 5385 | 147.1 | 182.7 |
| 25829 | 201.9 | 166.3 | 6173 | 159.5 | 165.1 |
| 25893 | 110.3 | 154.4 | 9009 | 103.7 | 149.4 |
| 37275 | 89.9 | 166.5 | 9187 | 117.2 | 153.9 |
| 37301 | 197.4 | 174.2 | 20133 | 205.3 | 154.1 |
| 25456 | 157.0 | 165.0 | 39737 | 147.0 | 145.0 |
| 28624 | 158.5 | 146.1 | | | |
| 28705 | 130.6 | 121.1 | | | |
| 35229 | 130.9 | 160.7 | | | |
| 39645 | 109.8 | 145.1 | | | |

[a]Here P is the magnitude of $\pi^0$ momentum.

[b]Here E is the muon total energy.

## APPENDIX IV

### Evaluation of Normalization Factors for $K^+_{e3}$, $K^+_{\mu 3}$ Distributions

A. $K^+_{e3}$

The normalization factor for $K^+_{e3}$ decay is defined by

$$R(K^+_{e3}) = A_e^{\,2} N_e(\lambda) = \int_0^{P^e_{max}} \int_{-1}^{+1} F_e^V(P, \theta) d\cos\theta \, dP$$

$$= A_e^{\,2} \int_0^{P^e_{max}} \frac{4}{3} \frac{P^4}{E} \left(1 + \lambda \frac{q^2}{m_\pi^{\,2}}\right)^2 dP ,$$

where $q^2 = W^2 - P^2 = M_K^{\,2} + m_\pi^{\,2} - 2M_K E$, $P^e_{max}$ is 228.5 MeV/c, and $R(K^+_{e3})$ is the $K^+_{e3}$ decay rate.

Explicit evaluation of this integral yields

$$N_e(\lambda) = (7.2013 + 26.58\lambda + 41.29\lambda^2) \times 10^8 \text{ MeV}^4.$$

B. $K^+_{\mu 3}$

The normalization factor for $K^+_{\mu 3}$ decay is defined by

$$R'(K^+_{\mu 3}) = A_\mu^{\,2} N_\mu(\lambda, \lambda'_\mu, \frac{B_\mu}{A_\mu}) = \int_0^{P^\mu_{max}} \int_{E_{\mu min}(P)}^{E_{\mu max}(P)} D(E_\mu) G^V(P, E_\mu) dE_\mu dP,$$

where $R'(K^+_{\mu 3})$ is the decay rate of $K^+_{\mu 3}$ satisfying geometrical and kinematic restrictions imposed on our $K^+_{\mu 3}$ sample; $m_\mu$, the muon mass, is 105.66 MeV; $P^\mu_{max}$ is 215.3 MeV/c; $E_{\mu min}(P) = [(W - P)^2 + m_\mu^{\,2}]/2(W - P)$; and $E_{\mu max}(P) = [(W + P)^2 + m_\mu^{\,2}]/2(W + P)$.

If we define

$$K_n(P) = \int_{E_{\mu\,min}(P)}^{E_{\mu\,max}(P)} D(E_\mu)\, E_\mu^{\,n-1}\, dE_\mu,$$

then

$$N_\mu(\lambda, \lambda'_\mu, \frac{B_\mu}{A_\mu}) = J_1 + J_2\lambda + J_3\lambda^2 + \frac{B_\mu}{A_\mu}\Big[J_4 + J_5(\lambda + \lambda'_\mu)$$

$$+ J_6\lambda\lambda'_\mu\Big] + \frac{B_\mu^{\,2}}{A_\mu}\Big[J_7 + J_8\lambda' + J_9\lambda'^{\,2}\Big],$$

where the $J_1, \ldots J_9$ are constants found respectively from

$$J_1 = 2\int_0^{P^\mu_{max}} \frac{P}{E}\Big[-4K_3 + 4WK_2 - (W^2 - P^2 - m_\mu^{\,2})K_1\Big]\, dP,$$

$$J_2 = 4\int_0^{P^\mu_{max}} \frac{P}{E}\,\frac{(M_K^{\,2} + m_\pi^{\,2} - 2M_K E)}{m_\pi^{\,2}}\Big[-4K_3 + 4WK_2 - (W^2 - P^2 - m_\mu^{\,2})K_1\Big]\, dP,$$

$$J_3 = 2\int_0^{P^\mu_{max}} \frac{P}{E}\,\frac{(M_K^{\,2} + m_\pi^{\,2} - 2M_K E)^2}{m_\pi^{\,4}}\Big[-4K_3 + 4WK_2 - (W^2 - P^2 - m_\mu^{\,2})K_1\Big]\, dP,$$

$$J_4 = 8\,\frac{m_\mu^{\,2}}{M_K}\int_0^{P^\mu_{max}} \frac{P}{E}\,(WK_1 - K_2)\, dP,$$

$$J_5 = 8 \frac{m_\mu^2}{M_K} \int_0^{P^\mu_{max}} \frac{P}{E} \frac{(M_K^2 + m_\pi^2 - 2M_K E)}{m_\pi^2} (W K_1 - K_2) dP,$$

$$J_6 = 8 \frac{m_\mu^2}{M_K} \int_0^{P^\mu_{max}} \frac{P}{E} \frac{(M_K^2 + m_\pi^2 - 2M_K E)^2}{m_\pi^4} (W K_1 - K_2) dP,$$

$$J_7 = 2 \frac{m_\mu^2}{M_K^2} \int_0^{P^\mu_{max}} \frac{P}{E} (W^2 - P^2 - m_\mu^2) K_1 \, dP,$$

$$J_8 = 4 \frac{m_\mu^2}{M_K^2} \int_0^{P^\mu_{max}} \frac{P}{E} \frac{(M_K^2 + m_\pi^2 - 2M_K E)}{m_\pi^2} (W^2 - P^2 - m_\mu^2) K_1 \, dP,$$

and

$$J_9 = 2 \frac{m_\mu^2}{M_K^2} \int_0^{P^\mu_{max}} \frac{P}{E} \frac{(M_K^2 + m_\pi^2 - 2M_K E)^2}{m_\pi^4} (W^2 - P^2 - m_\mu^2) K_1 \, dP.$$

These calculations have been done by computer, with the following results:

$J_1 = 2.6277 \times 10^8$
$J_2 = 16.303 \times 10^8$
$J_3 = 30.264 \times 10^8$
$J_4 = 1.0346 \times 10^8$
$J_5 = 3.9449 \times 10^8$
$J_6 = 17.250 \times 10^8$
$J_7 = 0.20478 \times 10^8$
$J_8 = 1.7641 \times 10^8$
$J_9 = 4.1837 \times 10^8$ .

## REFERENCES


1. A. Pais and S. B. Treiman, Phys. Rev. 105, 1616 (1957).
2. R. P. Feynman and M. Gell-Mann, Phys. Rev. 109, 193 (1958).
3. S. Weinberg, R. E. Marshak, S. Okubo, E. C. G. Sudarshan, and W. B. Teutsch, Phys. Rev. Letters 1, 25 (1958).
4. J. Bernstein and S. Weinberg, Phys. Rev. Letters 5, 481 (1960).
5. S. W. MacDowell, Phys. Rev. 116, 1047 (1959).
6. N. Brene, L. Egardt, and B. Qvist, Nuclear Phys. 22, 553 (1961).
7. D. Luers, I. S. Mittra, W. J. Willis, and S. S. Yamamoto, Phys. Rev. Letters 7, 255 (1961).
8. J. K. Bøggild, K. H. Hansen, J. E. Hooper, M. Scharff, and P. K. Aditya, Nuovo Cimento 19, 621 (1961); S. Taylor, G. Harris, J. Orear, J. Lee, and P. Baumel, Phys. Rev. 114, 359 (1959).
9. J. M. Dobbs, K. Lande, A. K. Mann, K. Reibel, F. J. Sciulli, H. Uto, D. H. White, and K. K. Young, Phys. Rev. Letters 8, 295 (1962).
10. H. Chew, Phys. Rev. Letters 8, 297 (1962).
11. T. F. Stubbs, H. Bradner, W. Chinowsky, G. Goldhaber, S. Goldhaber, W. Slater, D. M. Stork, and H. K. Ticho, Phys. Rev. Letters 7, 188 (1961); G. Goldhaber, S. Goldhaber, J. Kadyk, T. Stubbs, D. H. Stork, and H. K. Ticho, Lawrence Radiation Laboratory Internal Report UCID-1250, Feb. 1960 (unpublished).
12. John L. Brown, Xenon Bubble Chamber, in Proceedings of an International Conference on Instrumentation for High-Energy Physics, 1960 (Interscience Publishers, Inc., New York, 1961), p. 110.
13. B. P. Roe, D. Sinclair, J. L. Brown, D. A. Glaser, J. A. Kadyk, and G. H. Trilling, Phys. Rev. Letters 7, 346 (1961).

This report was prepared as an account of Government sponsored work. Neither the United States, nor the Commission, nor any person acting on behalf of the Commission:

A. Makes any warranty or representation, expressed or implied, with respect to the accuracy, completeness, or usefulness of the information contained in this report, or that the use of any information, apparatus, method, or process disclosed in this report may not infringe privately owned rights; or

B. Assumes any liabilities with respect to the use of, or for damages resulting from the use of any information, apparatus, method, or process disclosed in this report.

As used in the above, "person acting on behalf of the Commission" includes any employee or contractor of the Commission, or employee of such contractor, to the extent that such employee or contractor of the Commission, or employee of such contractor prepares, disseminates, or provides access to, any information pursuant to his employment or contract with the Commission, or his employment with such contractor.